The University of Sydney

School of Civil Engineering
Sydney NSW 2006
AUSTRALIA

http://www.civil.usyd.edu.au/

Wind Loading of Telecommunication Antennas and Head Frames

Research Report No R881

Graeme S Wood BEng PhD

January 2007

ISSN 1833-2781

The University of Sydney

School of Civil Engineering
http://www.civil.usyd.edu.au/

Wind Loading of Telecommunication Antennas and Head Frames

Research Report No R881

Graeme S Wood BEng PhD

January 2007

Abstract:
The base balance wind tunnel testing technique was used to determine the wind loading on a range of telecommunication antennas and head frames. The cross-wind and torsional components of the wind loading were typically small, and the along-wind drag force dominated the response. As more antennas were added to the head frame the peak along-wind drag typically increased. The magnitude of the increase is complex due to significant shielding effects.

Keywords:
Telecommunication antennas, wind loading, drag force, interference

Acknowledgements:
The experimental work described in this report was undertaken as an undergraduate thesis project. The extensive wind tunnel testing programme was conducted diligently by Ben Hawley and James Prosser.

The work was generously funded by Crown Castle.

Copyright Notice

g.wood@usyd.edu.au

ISSN 1833-2781

Published by:
School of Civil Engineering
The University of Sydney
Sydney NSW 2006
AUSTRALIA

January 2007

This report and other Research Reports published by the School of Civil Engineering are available on the Internet:

http://www.civil.usyd.edu.au

Table of Contents

1. Introduction

The top of typical telecommunication towers consist of a headframe with a number of antennas attached, Fig. 1. The headframe is generally a lightweight steel construction located at the top of the mast and is used for mounting multiple antennas and allowing access for maintenance. Antennas are typically elongated of circular cylindrical elements and mounted on the headframe or directly on the mast.

Estimation of the wind induced drag force on these structures is complicated due to both positive and negative interference effects. Current practice is to use proprietary wind tunnel results or use a wind loading standard, which has not been specifically written for such a complex task. (ASCE, 2002, British Standard, 1997, Standards Australia, 2002). When using these standards, designers typically sum the individual member drag force and apply an arbitrary shielding factor.

Fig. 1: Typical communication tower with antennas and headframe

Proprietary model and full scale wind tunnel tests have been conducted, but results have not been made freely available. As mentioned above, there are sections in wind loading standards which could be adapted to allow an estimation of the drag force on these structures, there is little referenced in the literature. The series of model tests described herein provides design information and guidance for estimating the along wind mean drag coefficients for different antenna configurations. Assuming quasi-steady theory, the mean drag coefficients can be scaled to prototype scale. The dynamic nature of communication towers was not investigated in this report, as this is primarily a function of the stiffness of the entire system,

2. Literature review

Literature on wind loading on antennas and head frames is reasonably limited, probably due to the apparent simple nature of the problem. Proprietary work has been conducted in determining the wind loads on specific structures, however little is freely and easily available in the public domain.

An in depth review of the wind loading on antennas and frame structures is given by Holmes (2001).

The drag force on basic cylindrical shapes can be readily estimated using information contained in most wind loading design standards (Standards Australia, 2002, ASCE, 2002, British Standard, 2002). The drag force on more complex shapes can be found in most fluid mechanic textbooks and ESDU, 1971, 1979. The drag for most antennas will lie somewhere between the values for a sharp-cornered rectangle and circular/elliptical section. Although easy to determine for the case where the wind is blowing orthogonal to an axis of symmetry; this becomes more difficult as the angle of attack changes. It was therefore considered important to test isolated antenna to give directional drag forces for standard antenna cross-sectional profiles.

Typical head frames can be divided into two categories; member (turret and Mercedes) and frames (square, triangular, and circular), Fig. 4. It is difficult to calculate the drag force on both types of head frames due to interference effects (both positive and negative) between closely spaced members. Interference has been studied extensively for specific cases including, ESDU, 1984, 1982a, Marchman and Werme, 1982, and can be significant for closely spaced items. ESDU 1982, indicates that for structural members whose spacing is greater than 10 times the width of the member normal to the wind direction, interference effects will be negligible. This would indicate that for the isolated circular, turret, and Mercedes head frames interference may be important, but for the square and triangular there would only be expected to be slight interference for the corner members. Evidently with the antenna attached interference effects will be more significant.

Wind loading on lattice frames and towers has been studied in some detail culminating in ESDU 1982b, 1981, Standards Australia, 1994, and British

Standard, 1986. The differences between a lattice tower and a telecommunication head frame include:

- a lattice tower is limited to a square or triangular plan shape,
- a lattice tower has an identical member pattern on all faces of the tower,
- a lattice tower has a significantly larger height:width ratio, and
- a lattice tower has few internal members.

The drag coefficient for a lattice tower is a function of the shape of the structural members (circular, or sharp edged), and the solidity of one face of the tower. The solidity is calculated as the ratio of the projected solid area of the members on one face of the tower to the total enclosed area of the tower section under consideration.

Later experimental work by Carril et al., 2003 showed that the code estimations generally yielded a good approximation to the measured wind loads. However, they concluded that the difference between the measured and code calculated predictions were due to the lateral members which increase the wind loading, but are not considered in the code calculation. This has a significant influence when extrapolating to head frames where there are a higher proportion of internal and lateral members in the structure.

Interference effects of microwave dish antennas have also been researched by Holmes et al. 1993 and Carrill et al. 2003. Both publications indicate that the wind load could increase by a factor of up to 30%. However, it should be noted that the microwave antenna tested were of a size equivalent to, or in excess of, the width of the tower. Applying the proposed interference factors, which are contained in the various design codes and standards to prismatic antennas mounted on head frames is likely to introduce significant inconsistencies.

In summary, there is little available information to aid the designer in determining the wind load on typical head frames with antennas. It is considered that the estimation of the wind loading on an isolated head frame would be best conducted by summing the drag forces on individual members. Interference effects are expected to be significant when antennas are connected to the head frame and an interference factor should be employed. However, the interference factor contained in the current codes and standards are for microwave dish antennas, which are of a similar size to the supporting lattice tower.

3. Experimental technique

Wind tunnel testing was conducted on 1:5 scale models mounted in the centre of the No. 1 boundary layer wind tunnel located in the School of Civil Engineering. The wind tunnel is approximately 2.4 m wide and 2.0 m high. The mean velocity and turbulence profiles are shown in Fig. 2 and show essentially uniform flow across the centre of the tunnel with a turbulence intensity of approximately 10%. The scale of turbulence is too small for models of this scale, but since the full-scale structures would be embedded in any air stream the quasi-steady assumption is assumed to apply.

Testing was conducted on three different antenna types, RFS DPS60, RFS APXV-18, and Argus JPX310D, Fig. 3, tested individually and mounted on five typical head frames: square, triangular, circular, turret and Mercedes, Fig. 4. All head frames were manufactured using circular hollow aluminium sections. Specific antenna layouts will be discussed in the relevant sections. The antennas are generally connected to the head frame via a mount, which consists of a vertical circular element in the order of 2.2 m long. The headframes were all constructed of circular members. The primary prototype dimensions of the antennas and head frames are given in Fig. 6 and Fig. 5, with full-scale drawings in Appendix 1.

The models were mounted on a six degree of freedom base balance in the free stream of the No. 1 boundary layer wind tunnel at The University of Sydney with the centre of rotation located in the centre of the support mast. The force and moment signals were recorded at 40 Hz for a period of 20 seconds. In accordance with telecommunication industry practice the mean along and cross wind drag forces have been divided by the mean dynamic pressure in the free stream at mid height of the model to give an ‘equivalent sail area’ (ESA), Eq. 1. The mean dynamic pressure was measured using a Pitot-static tube situated in the free stream at mid height of the model. Mean torque values have been expressed as an eccentricity based on the along-wind drag force, Eq. 2, which can then be expressed as a percentage of the frontal width of the head frame.

Equivalent Sail Area, $$\mathrm{ESA} = \frac{\overline{F}_d}{\frac{1}{2}\rho \cdot \overline{V}^2} \left(= C_d \cdot A_{ref}\right) \qquad [1]$$

Eccentricity, $$e_x = \frac{M_z}{F_x} \qquad [2]$$

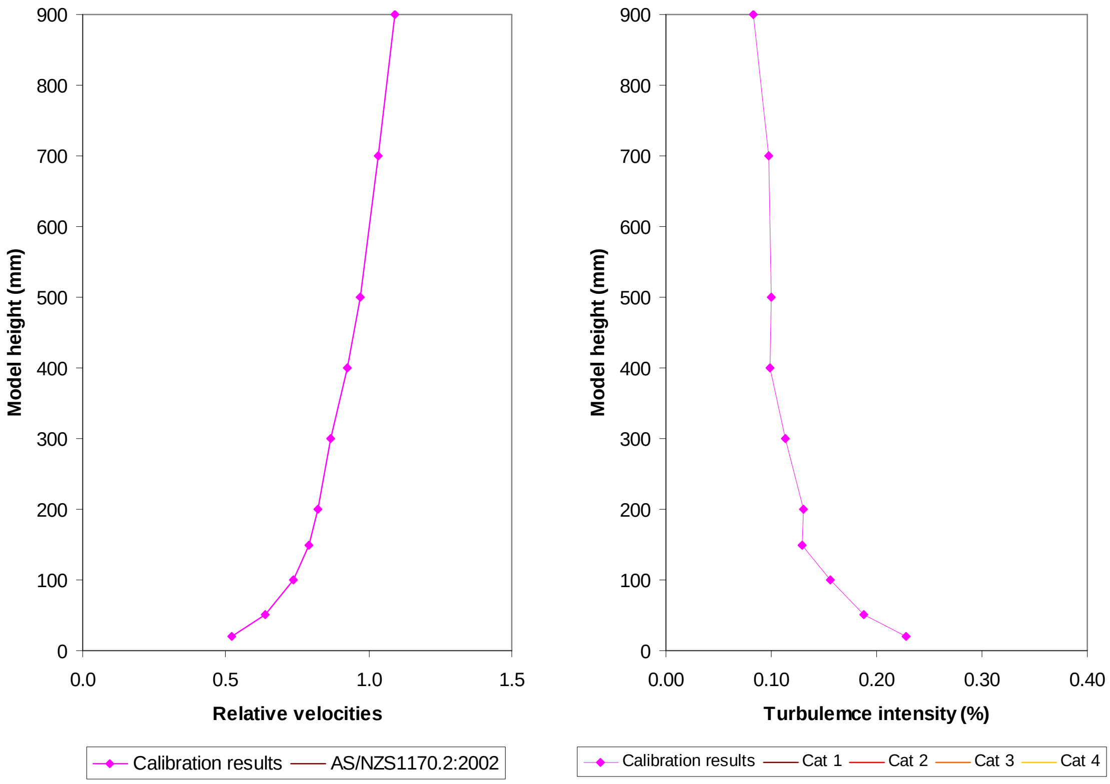

Fig. 2: Wind speed and turbulence profile in wind tunnel

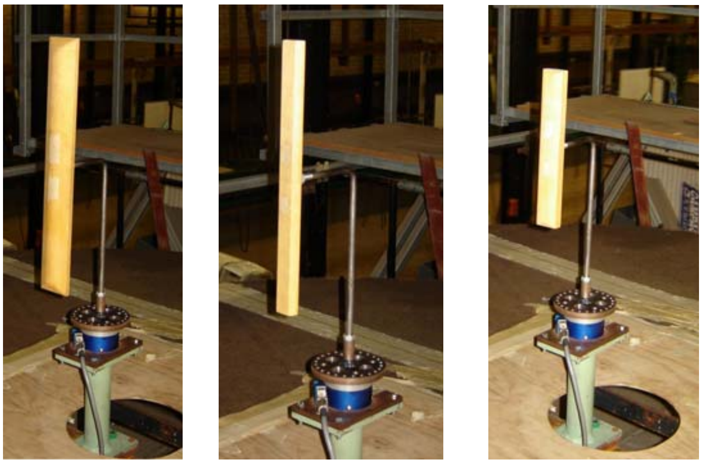

a. RFS DPS60 b. RFS APXV-18 c.JPX310D

Fig. 3: Photos of antennas tested

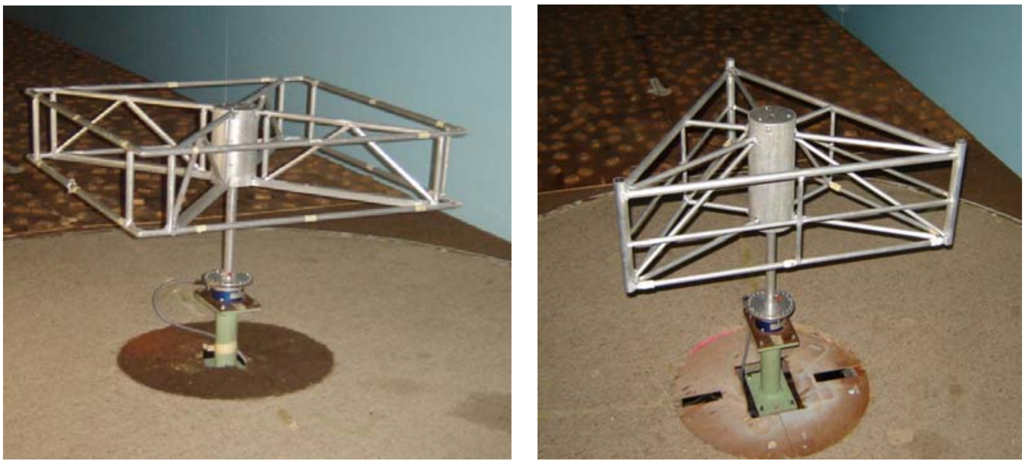

a. square b. triangular

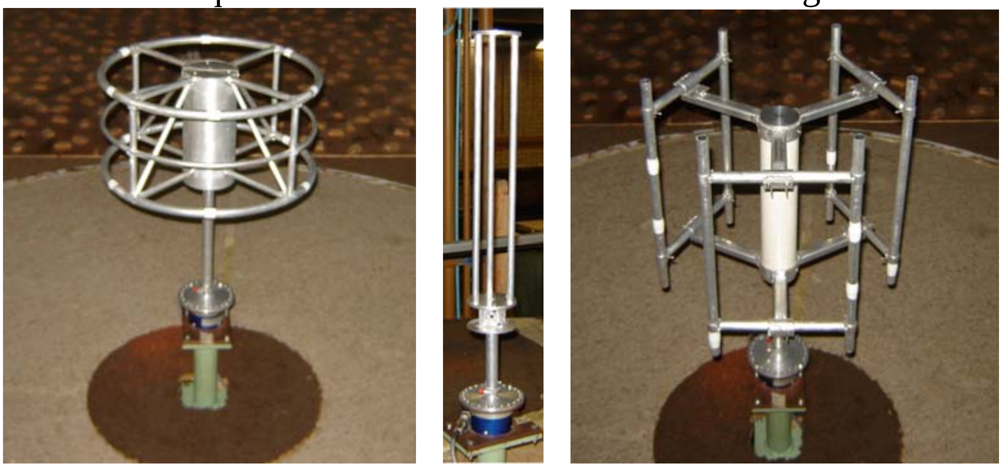

c. circular d. turret e. Mercedes

Fig. 4: Photos of head frames tested

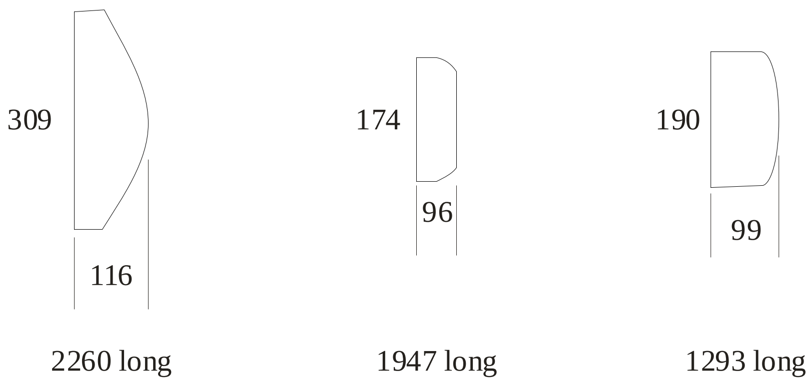

a. RFS DPS60 b. RFS APXV-18 c.JPX310D

Fig. 5: Schematic of antennas tested

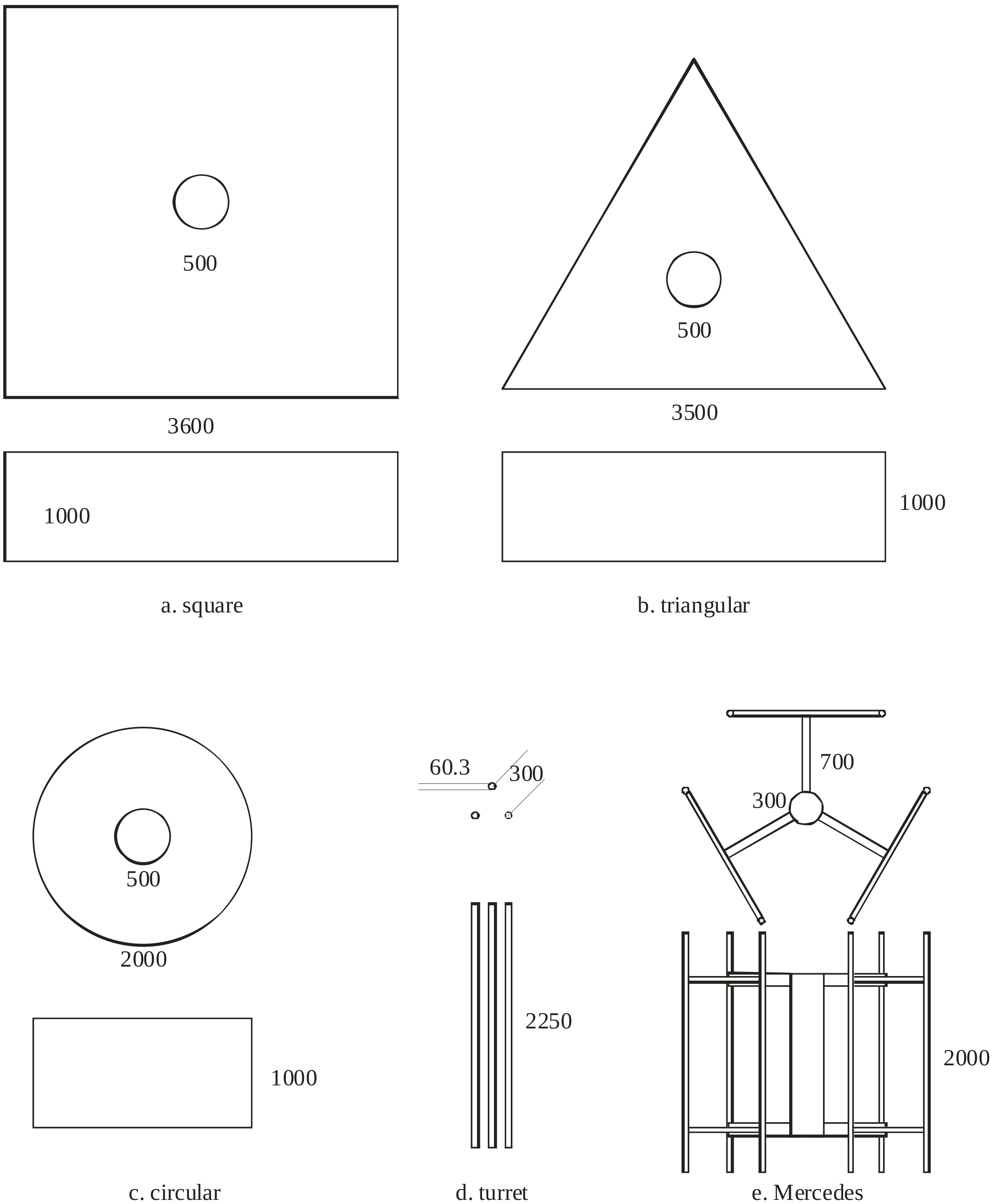

Fig. 6: Schematic of various head frames tested

4. Results

Reynolds number independence was investigated for individual panels and head frames. Typical results for the JPX310D antenna and the triangular head frame are shown in Fig. 7, where ESA is as defined in Eq. 1, and Reynolds number is defined in Eq. 3.

$$RN = \frac{\overline{V}.D}{\nu} \quad [3]$$

Where $\overline{V}$ is the mean free stream wind speed, D is a characteristic length taken as the width of the panel (38 mm) or the average diameter of the members (15 mm), and ν is the kinematic viscosity of air 1.5 x 10^{-5} m^2/s.

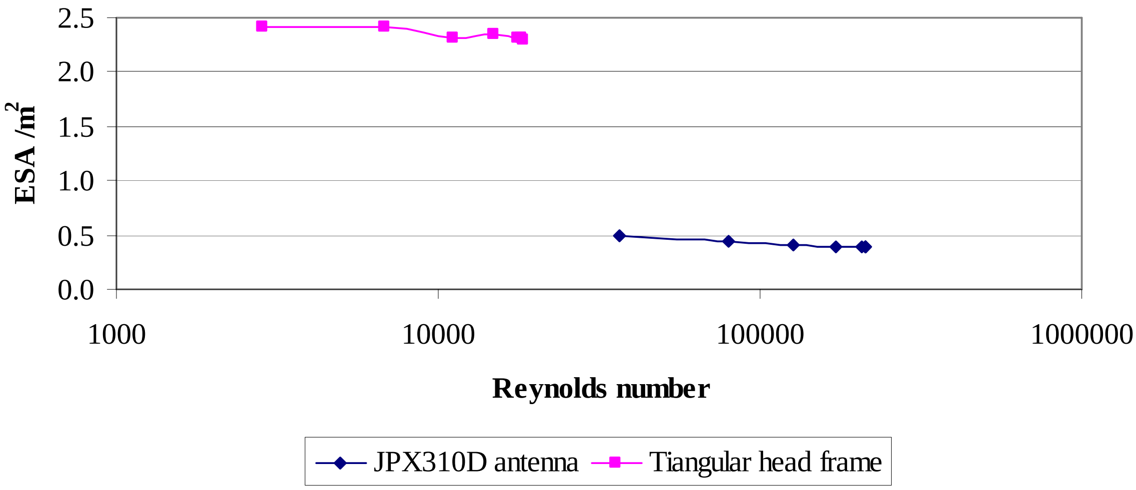

Fig. 7: Effective sail area versus Reynolds number

It is evident that the results are essentially independent of Reynolds number. It should be noted that these values of Reynolds number for the circular members would be classified as sub-critical according to Standards Australia AS/NZS1170.2:2002 Appendix E. All subsequent results are presented for a model wind speed of approximately 12 m/s.

4.1. Individual antennas

Individual antenna were mounted on a stand and tested on a six degree of freedom base balance, Fig. 3. Testing was carried out at 15° intervals, with the stand located to the lee of the panel to reduce interference effects. The axis notation for the tests is shown in Fig. 8. Along- (x) and cross-wind (y) effective sail areas as calculated by equation 1 are given in Fig. 9 for the isolated panels. The form of the graphs is similar for all panel types with the along wind ESA reasonably symmetric about 90°, but slightly higher in magnitude when the wind is blowing onto the rear of the panel due to the reduction in roundness of the body. The cross-wind ESA has a peak in the response when the wind is oblique to the curved portion of the antenna. As would be expected for this shape of body, the peak cross-wind ESA is lower than the along –wind ESA. Maximum along-wind ESA are given in Table 1.

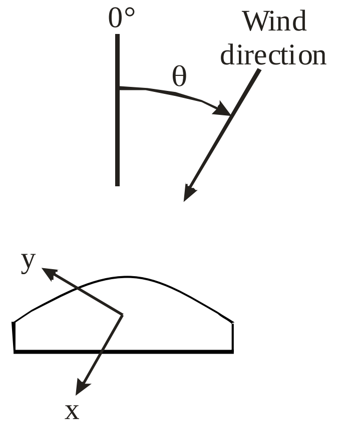

Fig. 8: Axis notation for individual panels

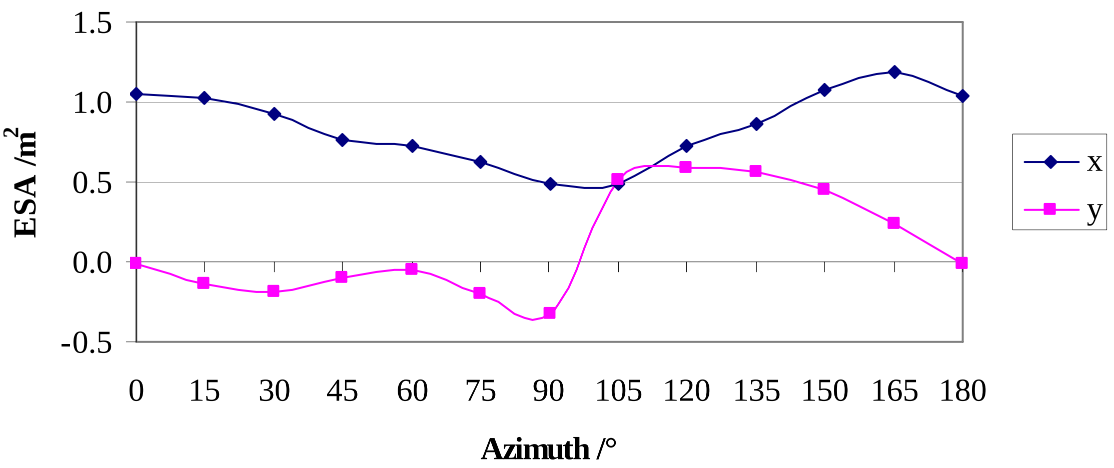

a. RFS DPS60

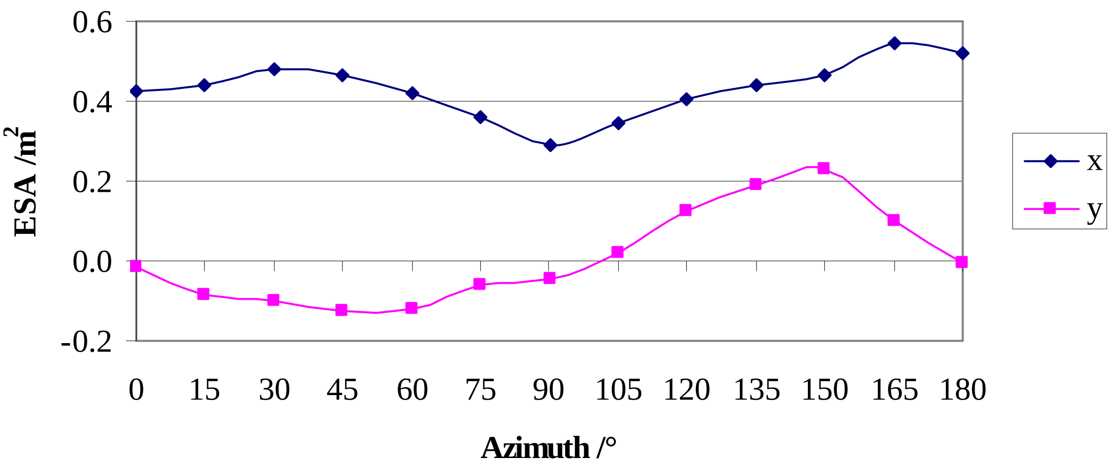

b. RFS APXV-18

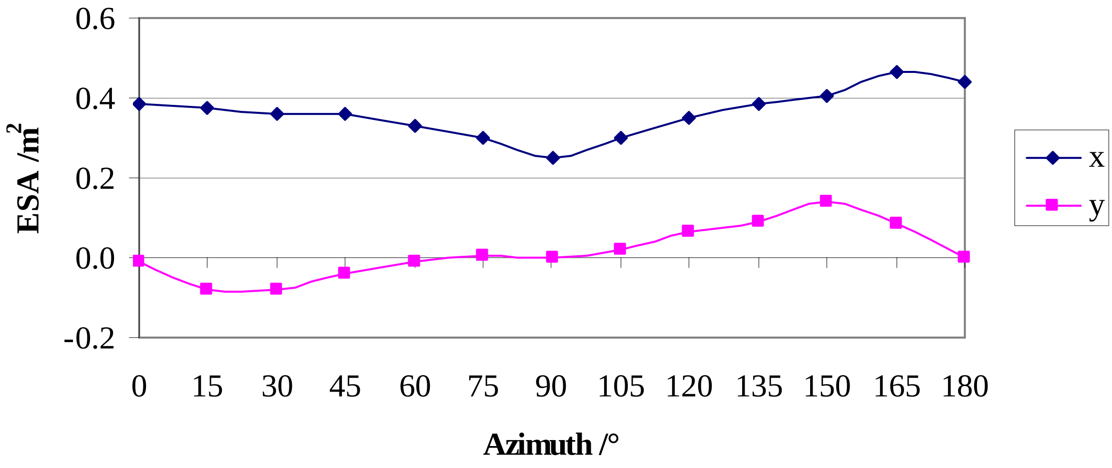

c.JPX310D

Fig. 9: Along and cross-wind effective sail areas for prototype individual panels

Panel	Max ESA_x /m^2
a large RFS DPS60-16ESX	1.2
b medium RFS APXV18-206517L	0.55
c small Argus JPX-310D	0.46

Table 1: Prototype max ESA for individual panels

4.2. Square head frame

All head frames were tested in isolation and in a number of commonly used antenna arrangements. Model antennas were connected to 400 mm long, 16 mm diameter (2 m long, 80 mm diameter at prototype scale) mounts clamped to the head frame. Dimensional details of the prototype head frame can be found in Appendix 1. Testing on the square head frame was carried out at 30° intervals. The panel layout, labelling system, and axis notation are shown in Fig. 10. The panel configurations tested are detailed in Table 2 and the Panel type (a, b, c) is from Table 1. The notation ‘30’ indicates the panel was rotated clockwise about the vertical axis of the mount by 30°, and the notation ‘m’ indicates a mount was attached without a panel, otherwise nothing was attached to the head frame at the location.

Fig. 11 shows the along-wind, cross-wind and torsional response, expressed as a percentage of the head frame width, of the square head frame with one large and one small panel mounted with the rear parallel to the head frame (0°) on each of three faces of the head frame. It is evident from Fig. 11 that the cross-wind component of the loading is small in comparison to the along-wind component;

this is true for all head frames tested and therefore will not be discussed further in this report. The torsional eccentricity is typically below 5% of the head frame width and will not be discussed further in this report.

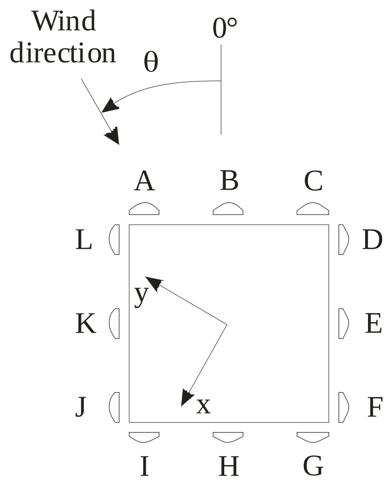

Fig. 10: Panel layout and axis notation for the square head frame

Directional along wind responses of the square head frame in the various configurations tested are shown in Fig. 12 to Fig. 19. It is unsurprising that an increase in the size or number of antennas increased the total drag force. However, the magnitude of the increase is complex due to the effects of shielding on the head frame members and the size and orientation of the downwind antennas. Flow visualisation showed that the position and offset of the antenna from the frame has a significant influence on the flow patterns and corresponding drag force. The degree of shielding to the elements behind the panels was significant.

The direction causing the peak along wind ESA changed depending on the antenna arrangement. Generally if the frame was relatively open the maximum drag occurred when the panels were to the rear of the head frame, when the sharper corners are pointing to the wind. With panels on more than one face the peak drag generally occurs when the wind is blowing normal to a set of panels on the windward face, and/or the panels are on the rear rather than the side. It is evident that the effect of pivoting the panels on the peak ESA measured is generally small.

Configuration	Panel A	B	C	D	E	F	G	H	I	J	K	L	Max ESA$_x$ /m^2
HF Only													3.3
2 Mounts	m		m										3.6
2 Large 1 Face 0°	a		a										4.5
2 Large 1 Face 30°	a30		a30										4.9
1 Large 1 Small 1 Face 0°	c		a										4.2
1 Large 1 Small 1 Face 30°	c30		a30										4.4
2 Small 1 Face 0°	c		c										4.1
2 Small 1 Face 30°	a		a										4.1
3 Mounts	m	m	m										3.9
3 Large 1 face 0°	a	a	a										5.2
3 Large 1 face 30°	a30	a30	a30										5.6
2 Large 1 Small 1 Face 0°	a	c	a										4.7
2 Large 1 Small 1 Face 30°	a30	c30	a30										5.2
3 Small 1 face 0°	c	c	c										4.3
3 Small 1 face 30°	c30	c30	c30										4.3
4 Mounts 2 Adj. Face	m		m							m		m	3.9
4 Large 2 Adj. Face 0°	a		a							a		a	5.4
4 Large 2 Adj. Face 30°	a30		a30							a30		a30	5.2
2 Large 2 Small 2 Adj. Face 0°	c		a							c		a	4.7
2 Large 2 Small 2 Adj. Face 30°	c30		a30							c30		a30	4.8
4 Small 2 Adj. Face 0°	c		c							c		c	4.2
4 Small 2 Adj. Face 30°	c30		c30							c30		c30	4.3
4 Mounts 2 Opp. Face	m		m				m		m				4.0
4 Large 2 Opp. Face 0°	a		a				a		a				5.6
4 Large 2 Opp. Face 30°	a30		a30				a30		a30				5.3
2 Large 2 Small 2 Opp. Face 0°	c		a				c		a				4.8
2 Large 2 Small 2 Opp. Face 30°	c30		a30				c30		a30				5.0
4 Small 2 Opp. Face 0°	c		c				c		c				4.6
4 Small 2 Opp. Face 30°	c30		c30				c30		c30				4.9
6 Mounts 2 Adj. Face	m	m	m							m	m	m	4.1
6 Large 2 Adj. Face 0°	a	a	a							a	a	a	6.1
6 Large 2 Adj. Face 30°	a30	a30	a30							a30	a30	a30	6.2
4 Large 2 Small 2 Adj. Face 0°	a	c	a							a	c	a	5.6
4 Large 2 Small 2 Adj. Face 30°	a30	c30	a30							a30	c30	a30	5.6
6 Small 2 Adj. Face 0°	c	c	c							c	c	c	4.6
6 Small 2 Adj. Face 30°	c30	c30	c30							c30	c30	c30	4.8
6 Mounts 2 Opp. Face	m	m	m				m	m	m				4.3
6 Large 2 Opp. Face 0°	a	a	a				a	a	a				6.7
6 Large 2 Opp. Face 30°	a30	a30	a30				a30	a30	a30				5.9
4 Large 2 Small 2 Opp. Face 0°	a	c	a				a	c	a				5.9
4 Large 2 Small 2 Opp. Face 30°	a30	c30	a30				a30	c30	a30				5.6
6 Small 2 Opp. Face 0°	c	c	c				c	c	c				5.2
6 Small 2 Opp. Face 30°	c30	c30	c30				c30	c30	c30				5.0
6 Mounts 3 Face	m		m	m		m				m		m	4.1
6 Large 3 Face 0°	a		a	a		a				a		a	6.2
6 Large 3 Face 30°	a30		a30	a30		a30				a30		a30	6.4
3 Large 3 Small 3 face 0°	c		a	c		a				c		a	5.5
3 Large 3 Small 3 face 30°	c30		a30	c30		a30				c30		a30	5.6
6 Small 3 Face 0°	c		c	c		c				c		c	4.8
6 Small 3 Face 30°	c30		c30	c30		c30				c30		c30	5.0
9 Mounts	m	m	m	m	m	m				m	m	m	4.5
9 Large 3 face 0°	a	a	a	a	a	a				a	a	a	7.4
9 Large 3 face 30°	a30	a30	a30	a30	a30	a30				a30	a30	a30	8.2
6 Large 3 Small 3 Face 0°	a	c	a	a	c	a				a	c	a	6.7
6 Large 3 Small 3 Face 30°	a30	c30	a30	a30	c30	a30				a30	c30	a30	7.1
9 Small 3 face 0°	c	c	c	c	c	c				c	c	c	5.5
9 Small 3 face 30°	c30	c30	c30	c30	c30	c30				c30	c30	c30	5.4

Table 2: Panel layout and max along-wind ESA for the square head frame

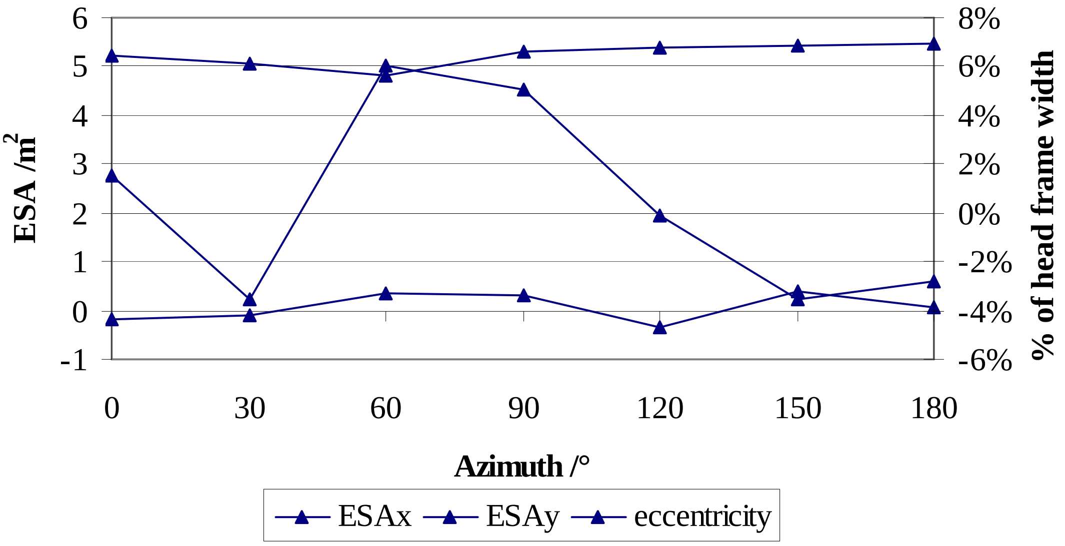

Fig. 11: Response of square headframe 3 large 3 small 3 face 0°

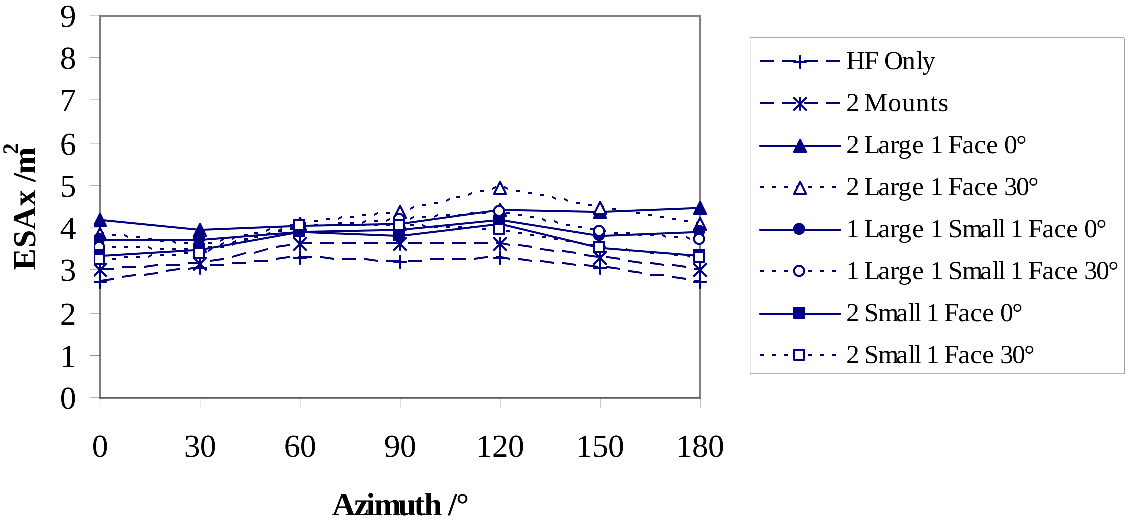

Fig. 12: Along wind response of square head frame with 2 antennas on one face

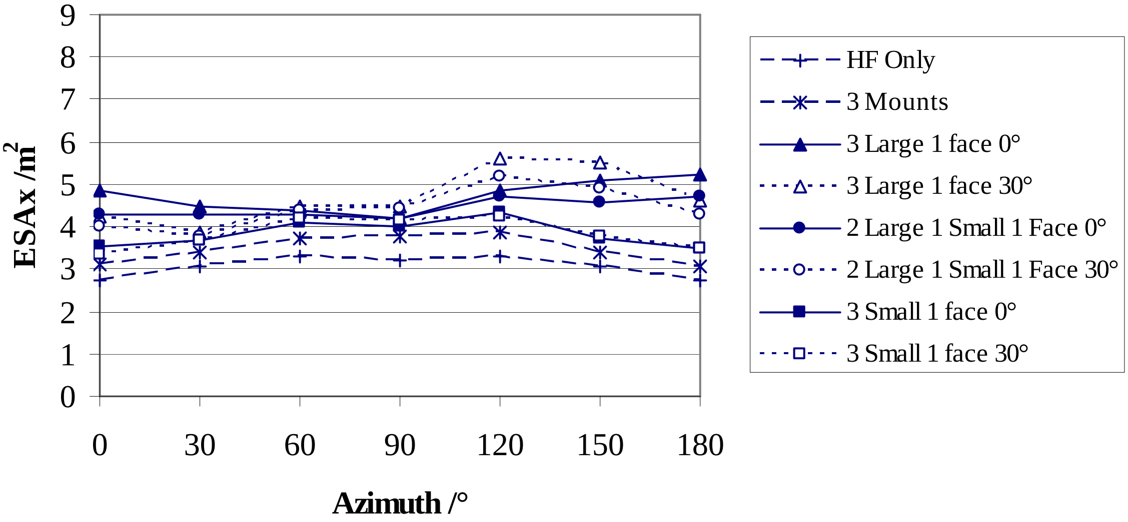

Fig. 13: Along wind response of square head frame; 3 antennas, one face

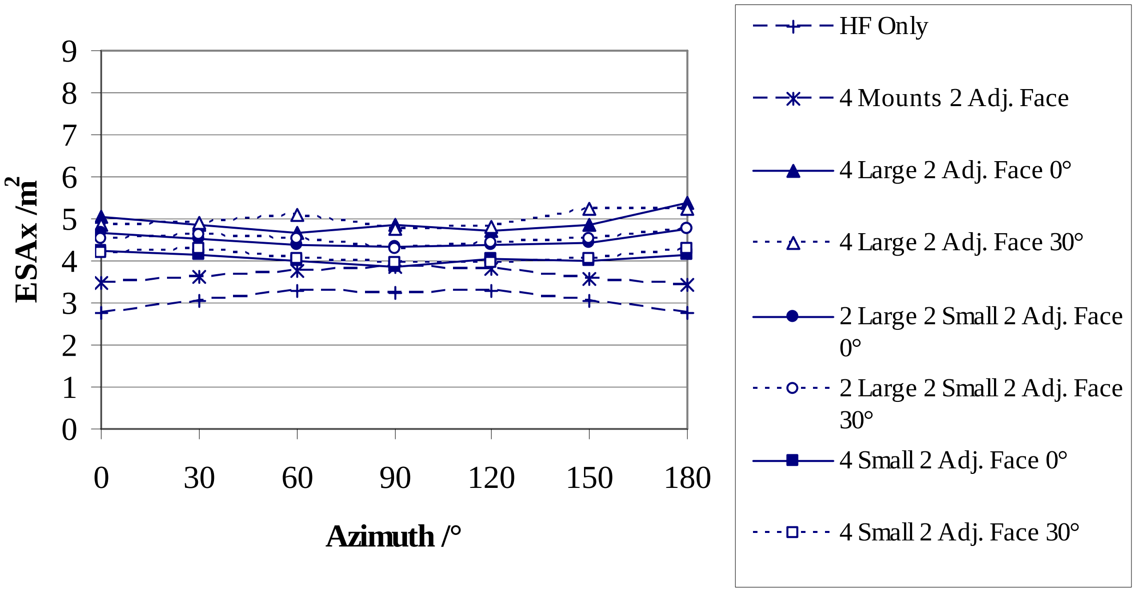

Fig. 14: Along wind response of square head frame; 4 antennas, 2 adjacent faces

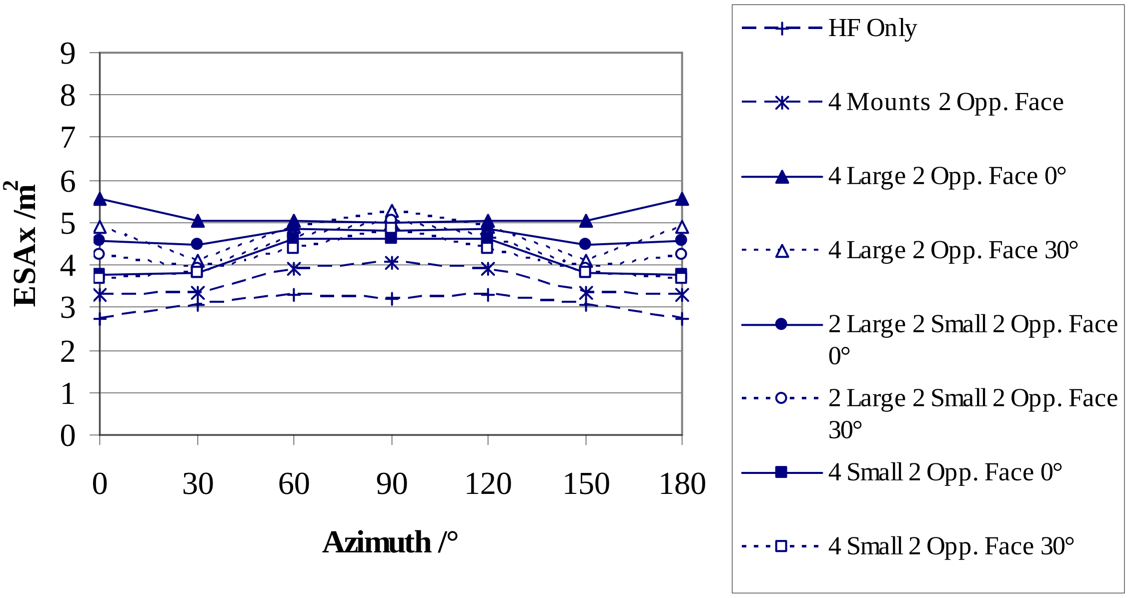

Fig. 15: Along wind response of square head frame; 4 antennas, opposite faces

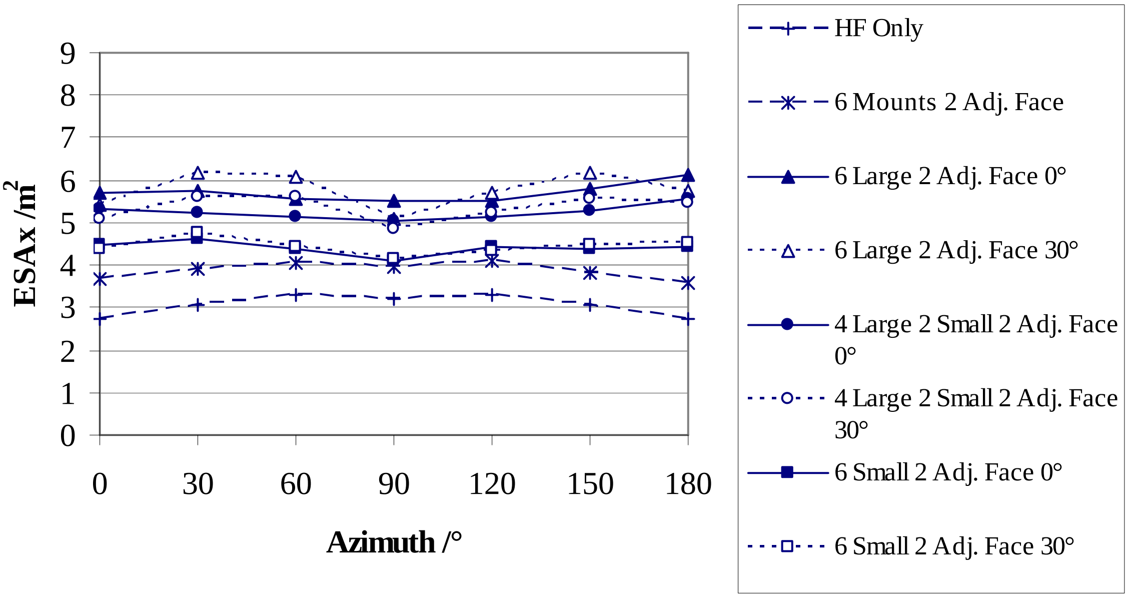

Fig. 16: Along wind response of square head frame; 6 antennas, 2 adjacent faces

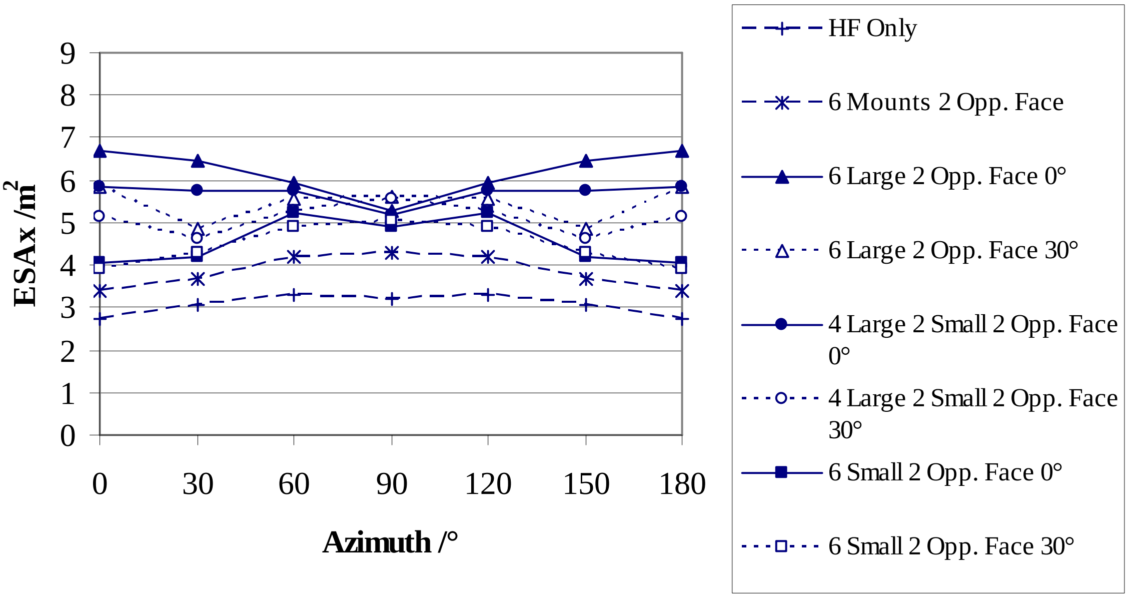

Fig. 17: Along wind response of square head frame; 6 antennas, opposite faces

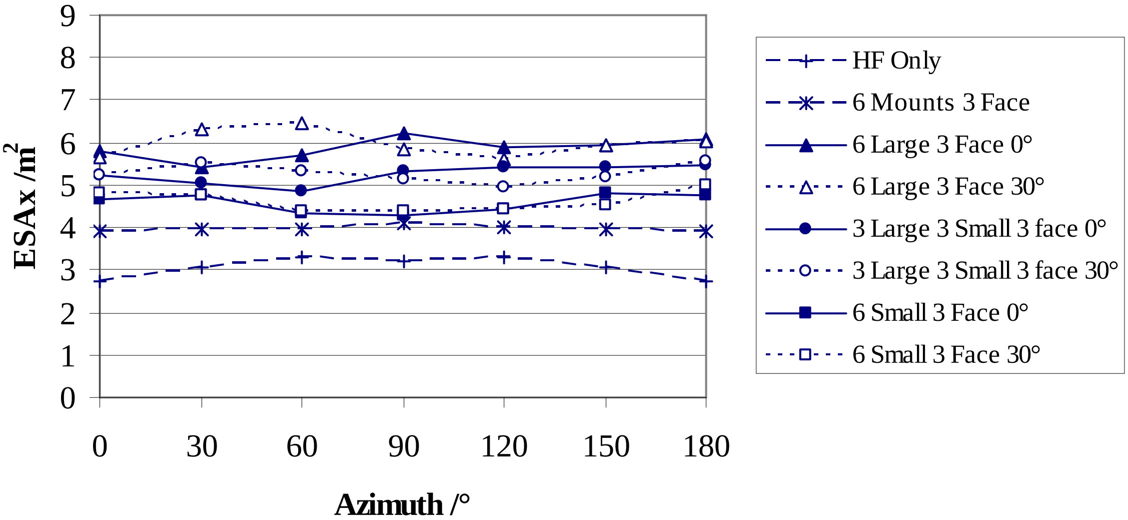

Fig. 18: Along wind response of square head frame; 6 antennas, 3 faces

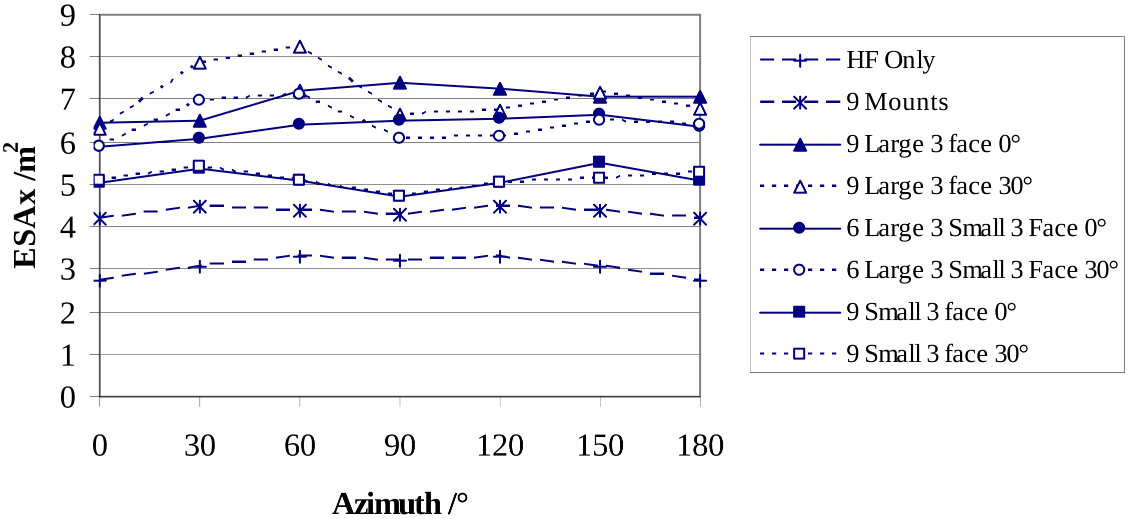

Fig. 19: Along wind response of square head frame; 9 antennas, 3 adjacent faces

4.3. Triangular head frame

Testing on the triangular head frame was carried out at 15° intervals up to 120°. The panel layout, labelling system, and axis notation are shown in Fig. 20. The panel configurations tested are detailed in Table 3 and the Panel type (a, b, c) is from Table 1. The notation '30' indicates the panel was rotated clockwise about the vertical axis of the mount by 30°, and the notation 'm' indicates a mount was attached without a panel.

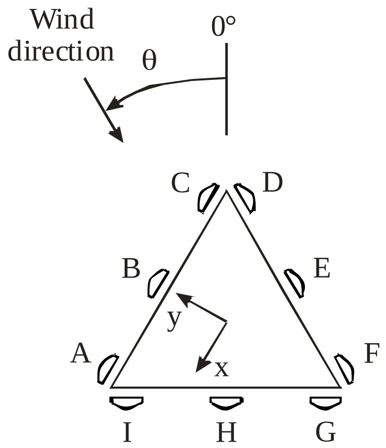

Fig. 20: Panel layout and axis notation for the triangular head frame

Configuration	Panel A	B	C	D	E	F	G	H	I	Max ESA_x /m^2
HF Only										2.4
Kick Plate										2.5
9 Mounts	m	m	m	m	m	m	m	m	m	3.6
6 Large 0°	a	m	a	a	m	a	a	m	a	5.7
6 Large 30°	a30	m	a30	a30	m	a30	a30	m	a30	5.7
6 Small 0°	c	m	c	c	m	c	c	m	c	4.5
6 Small 30°	c30	m	c30	c30	m	c30	c30	m	c30	4.3
9 Large 0°	a	a	a	a	a	a	a	a	a	6.5
9 Large 30°	a30	a30	a30	a30	a30	a30	a30	a30	a30	6.5
6 Large 3 Small 0°	a	c	a	a	c	a	a	c	a	6.1
6 Large 3 Small 30°	a30	c30	a30	a30	c30	a30	a30	c30	a30	6.0
9 Small 0°	c	c	c	c	c	c	c	c	c	4.8
9 Small 30°	c30	c30	c30	c30	c30	c30	c30	c30	c30	4.5

Table 3: Panel layout and max along-wind ESA for the triangular head frame

Directional along wind responses of the triangular head frame in the various configurations tested are shown in Fig. 21 and Fig. 22. It is unsurprising that an increase in the size or number of antennas increased the total drag force. However, the magnitude of the increase is complex due to the effects of shielding on the head frame members and the size and orientation of the downwind antennas. Flow visualisation showed that the position and offset of the antenna from the frame has a significant influence on the flow patterns and corresponding drag force. The degree of shielding to the elements behind the panels was significant.

The along-wind ESA was reasonably independent of wind direction, but the peak response generally occurred when the wind was blowing normal to a face of the triangle. Again the effect of pivoting the antennas was minimal.

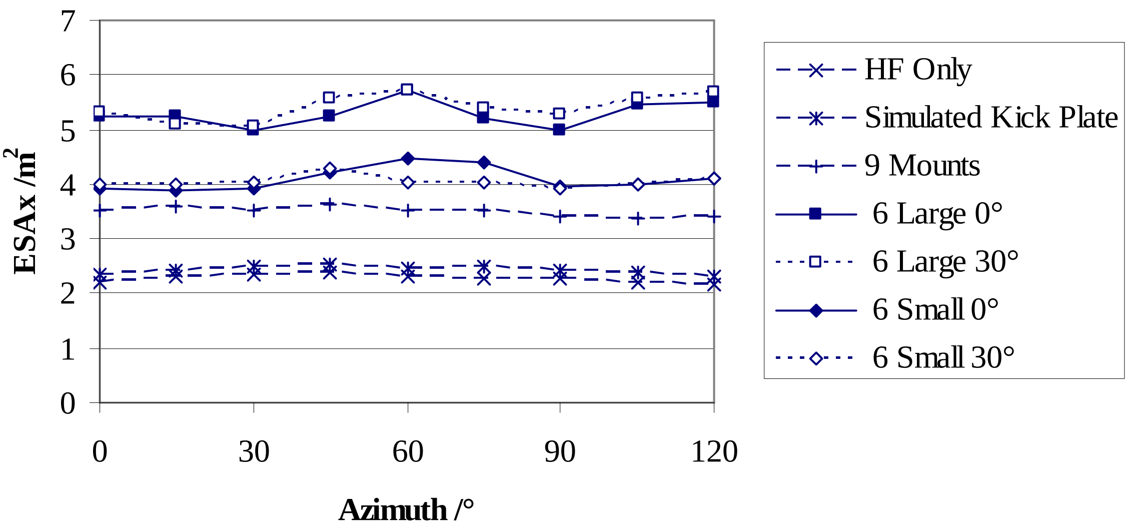

Fig. 21: Along wind response of the triangular head frame with 6 antennas

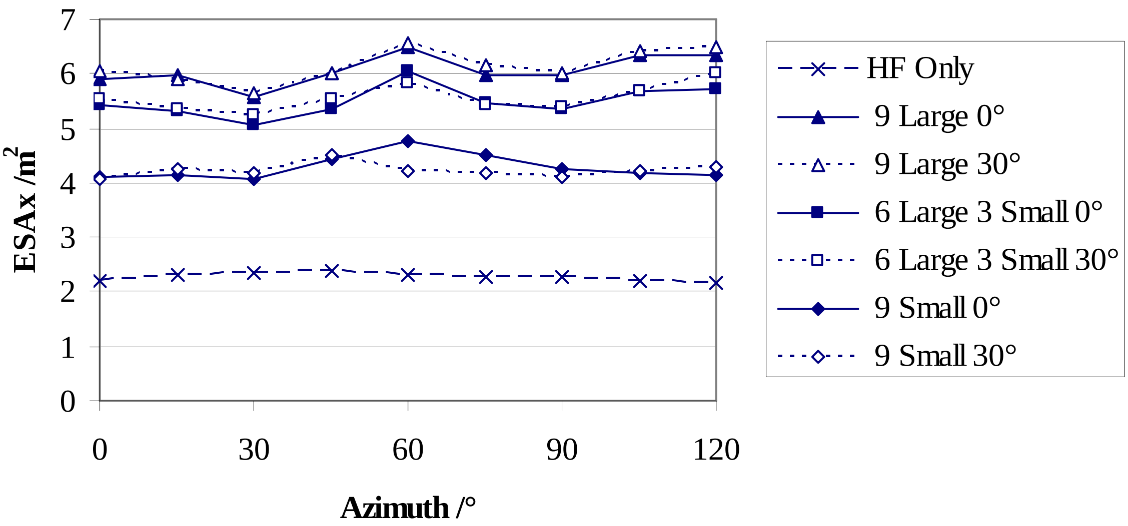

Fig. 22: Along wind response of the triangular head frame with 9 antennas

4.4. Circular head frame

Testing on the circular head frame was carried out at 30° intervals up to 120°. The panel layout, labelling system, and axis notation are shown in Fig. 23. The panel configurations tested are detailed in Table 4 and the Panel type (a, b, c) is from Table 1. The notation '30' indicates the panel was rotated clockwise about the vertical axis of the mount by 30°, the notation 'm' indicates a mount was attached without a panel, and no entry indicates there was nothing attached to the head frame.

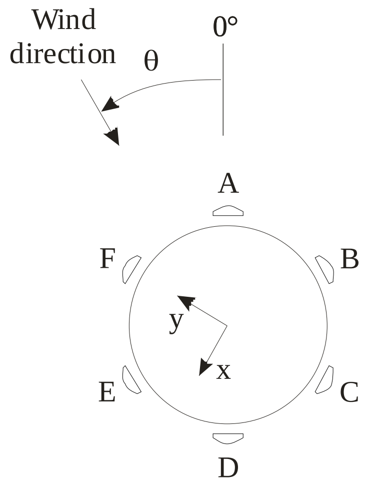

Fig. 23: Panel layout and axis notation for the circular head frame

Configuration	Panel A	B	C	D	E	F	Max ESA_x /m^2
HF Only							1.6
3 Mounts		m		m		m	2.1
3 Large 0°		a		a		a	3.2
3 Large 30°		a30		a30		a30	3.3
3 Small 0°		c		c		c	2.5
3 Small 30°		c30		c30		c30	2.4
6 Mounts	m	m	m	m	m	m	2.5
6 Large 0°	a	a	a	a	a	a	4.3
6 Large 30°	a30	a30	a30	a30	a30	a30	4.5
6 Small 0°	c	c	c	c	c	c	2.9
6 Small 30°	c30	c30	c30	c30	c30	c30	3.1

Table 4: Panel layout and max along-wind ESA for the circular head frame

Directional along wind responses of the circular head frame in the various configurations tested are shown in Fig. 24. It is unsurprising that an increase in the size or number of antennas increased the total drag force. However, the magnitude of the increase is complex due to the effects of shielding on the head frame members and the size and orientation of the downwind antennas. The along-wind ESA was reasonably independent of wind direction. Generalisations regarding wind direction are difficult for this head frame as the structural and antenna layouts were not symmetrical. Again the effect of pivoting the antennas was minimal.

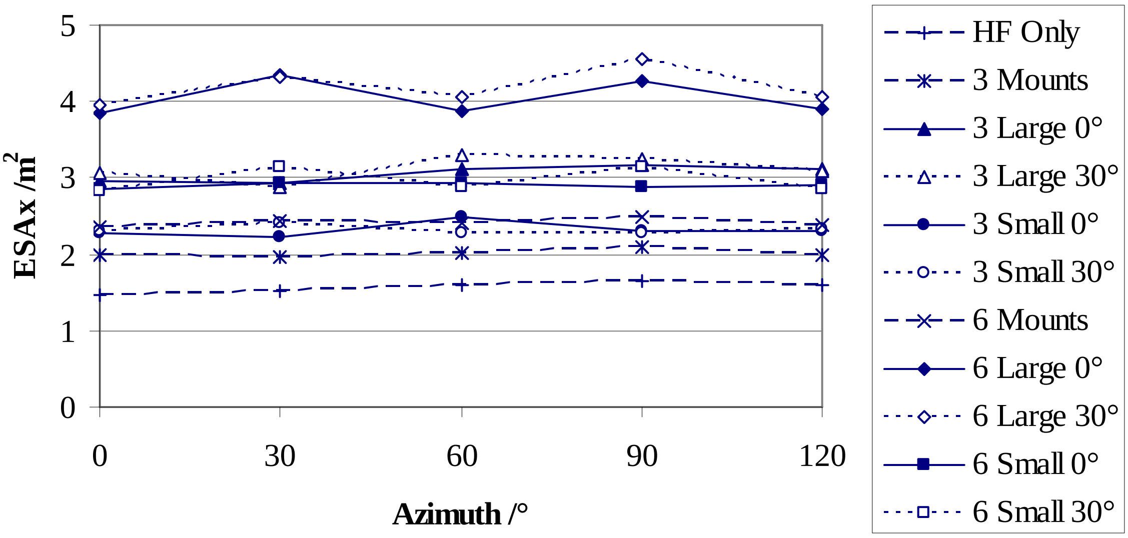

Fig. 24: Along wind response of the circular head frame

4.5. Turret head frame

Testing on the turret head frame was carried out at 15° intervals up to 120°. The panel layout, labelling system, and axis notation are shown in Fig. 25. The panel configurations tested are detailed in Table 5 and the Panel type (a, b, c) is from Table 1. The notation '30' indicates the panel was rotated clockwise about the vertical axis of the mount by 30°.

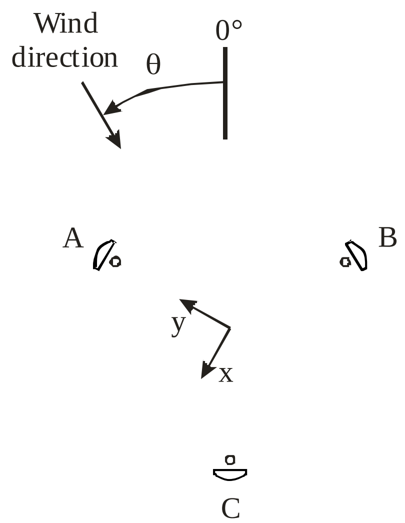

Fig. 25: Panel layout and axis notation for the turret head frame

Configuration	Panel A	Panel B	Panel C	Max ESA_x /m^2
HF Only				0.73
3 Large 0°	a	a	a	1.8
3 Large 30°	a30	a30	a30	1.8
3 Small 0°	c	c	c	1.2
3 Small 30°	c30	c30	c30	1.1

Table 5: Panel layout and max along-wind ESA for the turret head frame

Directional along wind responses of the turret head frame in the various configurations tested are shown in Fig. 26. It is unsurprising that an increase in the size or number of antennas increased the total drag force. The simple nature of this head frame makes it much more predictable in the wind, but there are still complex shielding issues. The along-wind ESA was reasonably independent of wind direction. The peak ESA occurred when the antennas were symmetric to the wind, and depended on the shape of the antennas.

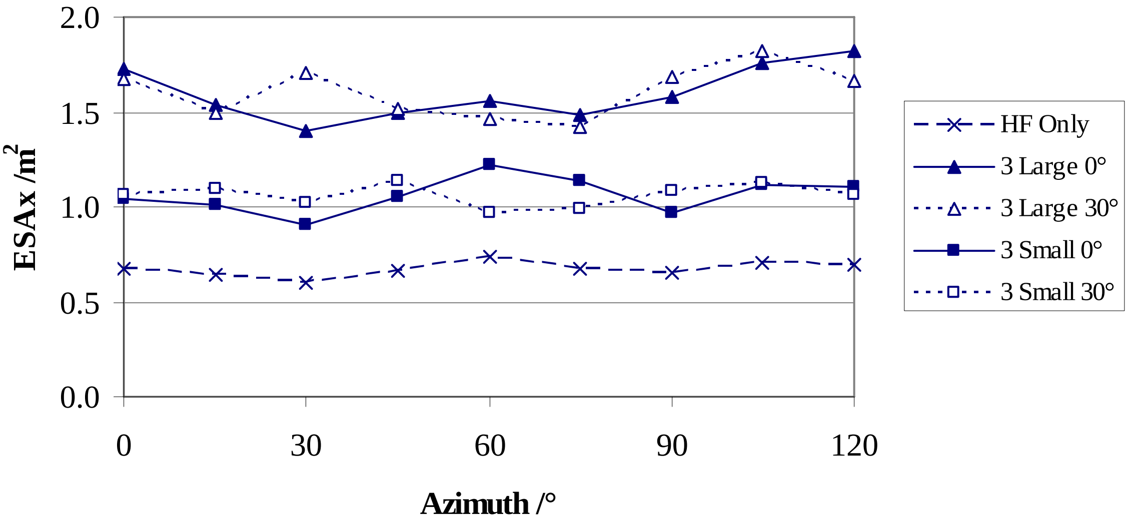

Fig. 26: Along wind response of the turret head frame

4.6. Mercedes head frame

Testing on the Mercedes head frame was carried out at 15° intervals up to 120°. The panel layout, labelling system, and axis notation are shown in Fig. 27. The panel configurations tested are detailed in Table 6 and the Panel type (a, b, c) is from Table 1. The notation '30' indicates the panel was rotated clockwise about the vertical axis of the mount by 30°, the notation 'm' indicates a mount was attached without a panel.

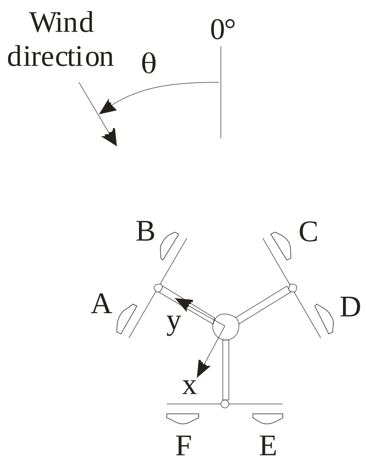

Fig. 27: Panel layout and axis notation for the Mercedes head frame

Configuration	Panel A	B	C	D	E	F	Max ESA_x /m^2
6 mounts	m	m	m	m	m	m	1.9
3 Large 0°	m	a	m	a	m	a	3.0
3 Large 30°	m	a30	m	a30	m	a30	3.0
3 Small 0°	c	m	c	m	c	m	2.4
3 Small 30°	c30	m	c30	m	c30	m	2.3
6 Large 0°	a	a	a	a	a	a	4.1
6 Large 30°	a30	a30	a30	a30	a30	a30	4.2
3 Large 3 Small 0°	c	a	c	a	c	a	3.6
3 Large 3 Small 30°	c30	a30	c30	a30	c30	a30	3.5
6 Small 0°	c	c	c	c	c	c	3.0
6 Small 30°	c30	c30	c30	c30	c30	c30	2.7

Table 6: Panel layout and max along-wind ESA for the Mercedes head frame

Directional along wind responses of the Mercedes head frame in the various configurations tested are shown in Fig. 28. It is unsurprising that an increase in the size or number of antennas increased the total drag force. The distribution of ESA with direction is more consistent for this head frame with the peak occurring when the wind is blowing from 60°; the wind normal to the front face of a pair of panels on the same mounting frame.

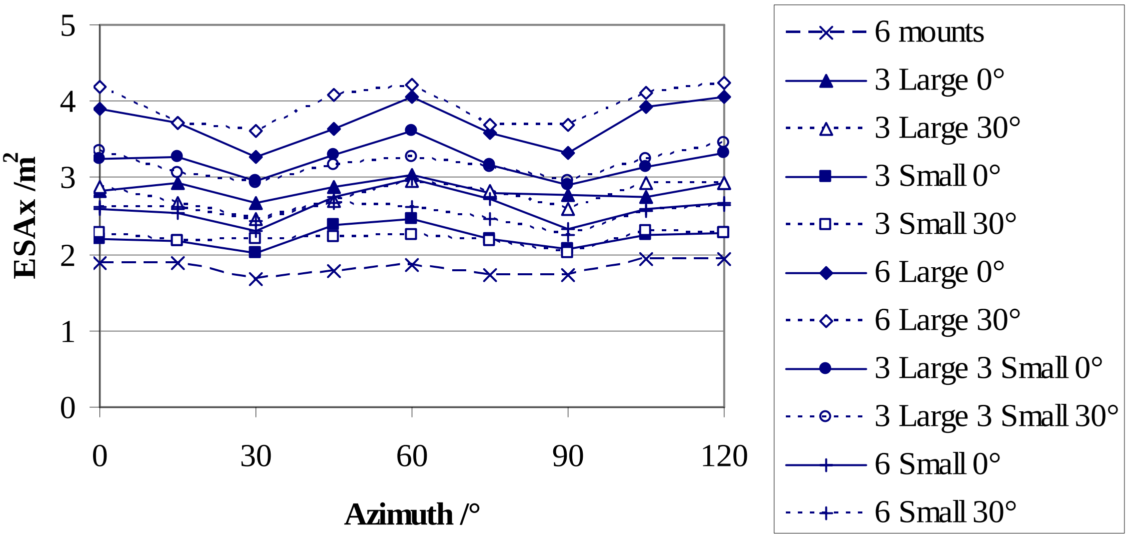

Fig. 28: Along wind response of the Mercedes head frame

5. Conclusions

This paper presents the results from simple drag force experiments on a range of standard telecommunication antennas and head frames tested in isolation and in a variety of antenna mounting configurations. The along-wind drag coefficients are reasonably independent of wind direction, but from the directional results and flow visualisation it is evident that shielding effects are complex and significant. The mean cross-wind component is typically about an order of magnitude lower than the along-wind component. The torsional component is generally small and could be estimated by applying the along-wind drag at an eccentricity of about 5% of the frontal width of the head frame.

6. References

ASCE, 2002, Minimum Design Loads for Buildings and Other Structures, ASCE 7-02.

British Standard, 1986, Lattice towers and masts: Code of practice for loading BS 8100-1:1986.

British Standard, 2002, Loading for buildings – Part 2: Code of practice for wind loads, BS6399.

Carrill, Jr., C.F., Isyumov, N., & Brasil, R., 2003, Experimental study of the wind forces on rectangular latticed communication towers with antennas, Journal of Wind Engineering and Industrial Aerodynamics, Vol.91, pp.1007-1022.

ESDU 1971, Fluid forces, pressures and moments on rectangular blocks, Engineering Sciences Data Item 71016.

ESDU, 1979, Mean fluid forces and moments on cylindrical structures: polygonal sections with rounded corners including elliptical shapes, Engineering Sciences Data Item 79026.

ESDU 1981, Lattice structures: Part 2: Mean fluid forces on tower-like space frames, Engineering Sciences Data Item, 81028.

ESDU, 1982a, Structural members: mean fluid forces on members of various cross sections, Engineering Sciences Data Item, 82007.

ESDU 1982b, Lattice structures: Part 1: Mean fluid forces on single and multiple plane frames, Engineering Sciences Data Item, 81027.

ESDU, 1984, Cylinder groups: mean forces on pairs of long circular cylinders, Engineering Sciences Data Item, 84015.

Holmes, J.D., Banks, R.W., & Roberts, G., 1993, Drag and aerodynamic interference on microwave dish antennas and their supporting towers, Journal of Wind Engineering and Industrial Aerodynamics, Vol.50, pp.263-270.

Holmes, J.D., 2001, Wind loading of structures, Spon Press.

Marchman III, J.F., & Werme, T.D., Mutual interference drag on signs and luminaires, Journal of the Structural Division, Proc. ASCE, Vol. 108, pp2235-2244.

Standards Australia, 1984, Design of steel lattice towers and masts, AS3995.

Standards Australia, 2002, Structural design actions, Part 2: Wind actions, AS/NZS1170.2

Appendix 1: Prototype antenna and head frame specifications

RFS DPS60 Antenna

RFS Radio Frequency Systems Pty Limited A.B.N. 99-004 686 097

Installation Instruction

CELLULAR ANTENNA
2.3 m PANEL

Doc No 28806E002
Issue 2
Page 1 of 3

MODEL : APXV906514 or DPS60-16ESX
FREQUENCY : 824 - 960 MHz
PANEL SIZE : 2.3 m

DESCRIPTION

The APXV906514 or DPS60-16ESX series are dual polarized directional sector antennas for polarization diversity systems. Refer to *Figure 1* for Antenna Details.

Individual connectors allow access to either + 45° or - 45° polarized radiators. Refer to *Figure 2* for Antenna Polarization.

The radiator structure is contained within a rectangular aluminium case covered by a UV stabilized plastic radome, which can be painted if required.

The aluminium case acts as a reflector, and gives the 65° azimuth beam width for both polarizations.

The antennas are supplied with variable electrical downtilt, which allows continuous adjustment between 2° and 8° by means of a graduated dial at the rear of the panel.

The control unit studs are reserved for a control unit, which can be mounted over the dial spindle, to enable remote adjustment of electrical downtilt.

The mounting kit, (including the mechanical tilt option) and installation for 1.3 m and 2.3 m panels are described in installation instruction Doc No 29460E000.

The input impedance of both polarizations is 50 ohms, with a return loss of greater than 18 dB over both AMPS and GSM frequency bands. The maximum input power is 500 watts.

The two connectors are 7-16 bulkhead connectors located on the rear of the panel. Each connector is labelled showing its polarization. Refer to *Figure 5.*

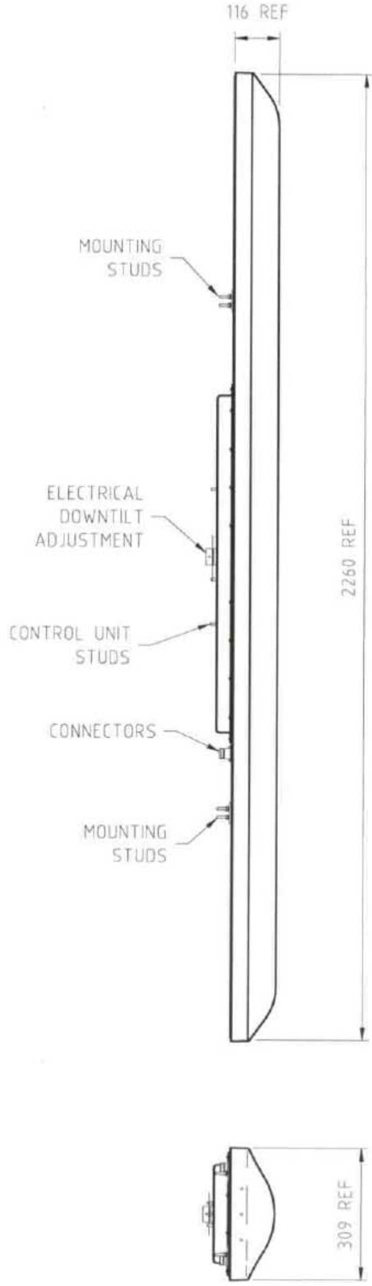

Figure 1 Antenna Details

Radio Frequency Systems Pty Limited
36 Garden Street, Kilsyth, Victoria, Australia, 3137
Tel: +61 3 9751 8400 Fax: +61 3 9761 5711
www.rfsworld.com

RFS APXV-18 Antenna

APx V18 - 206517L

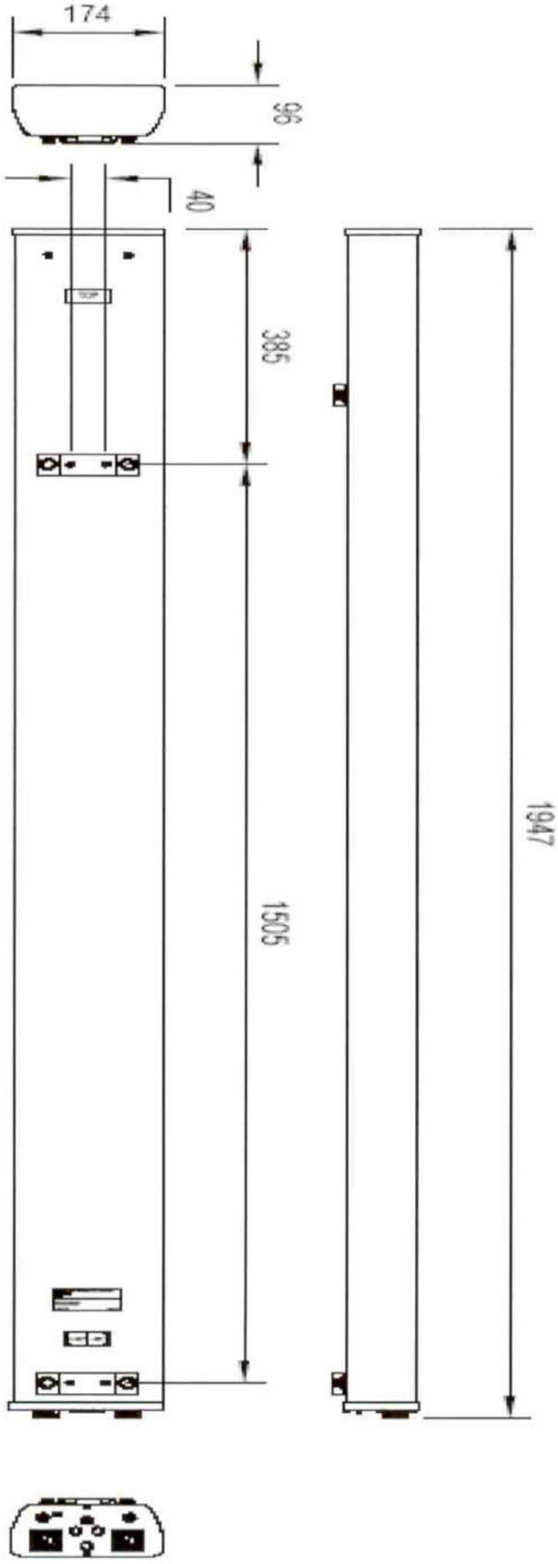

Argus JPX310D Antenna

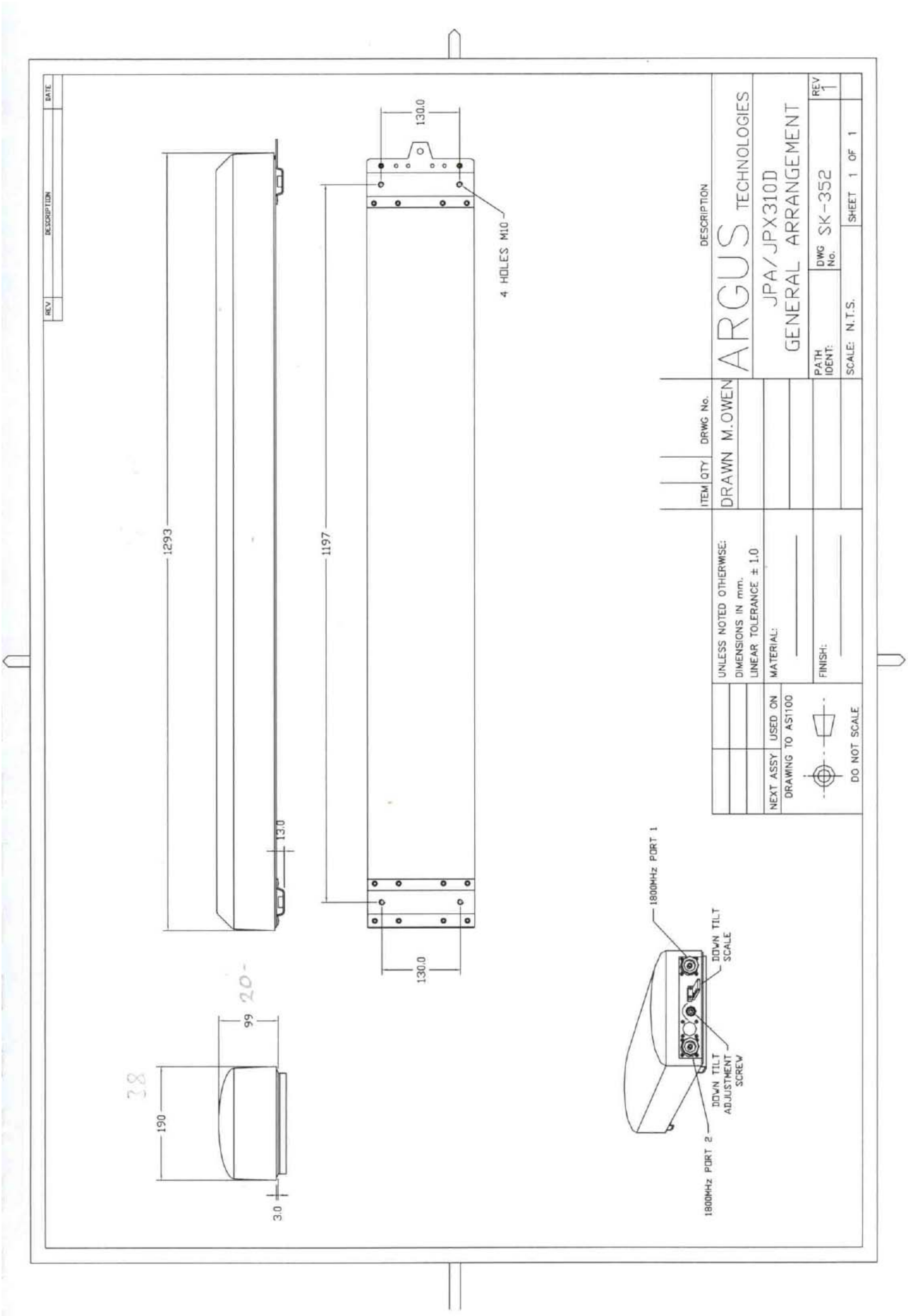

Square head frame

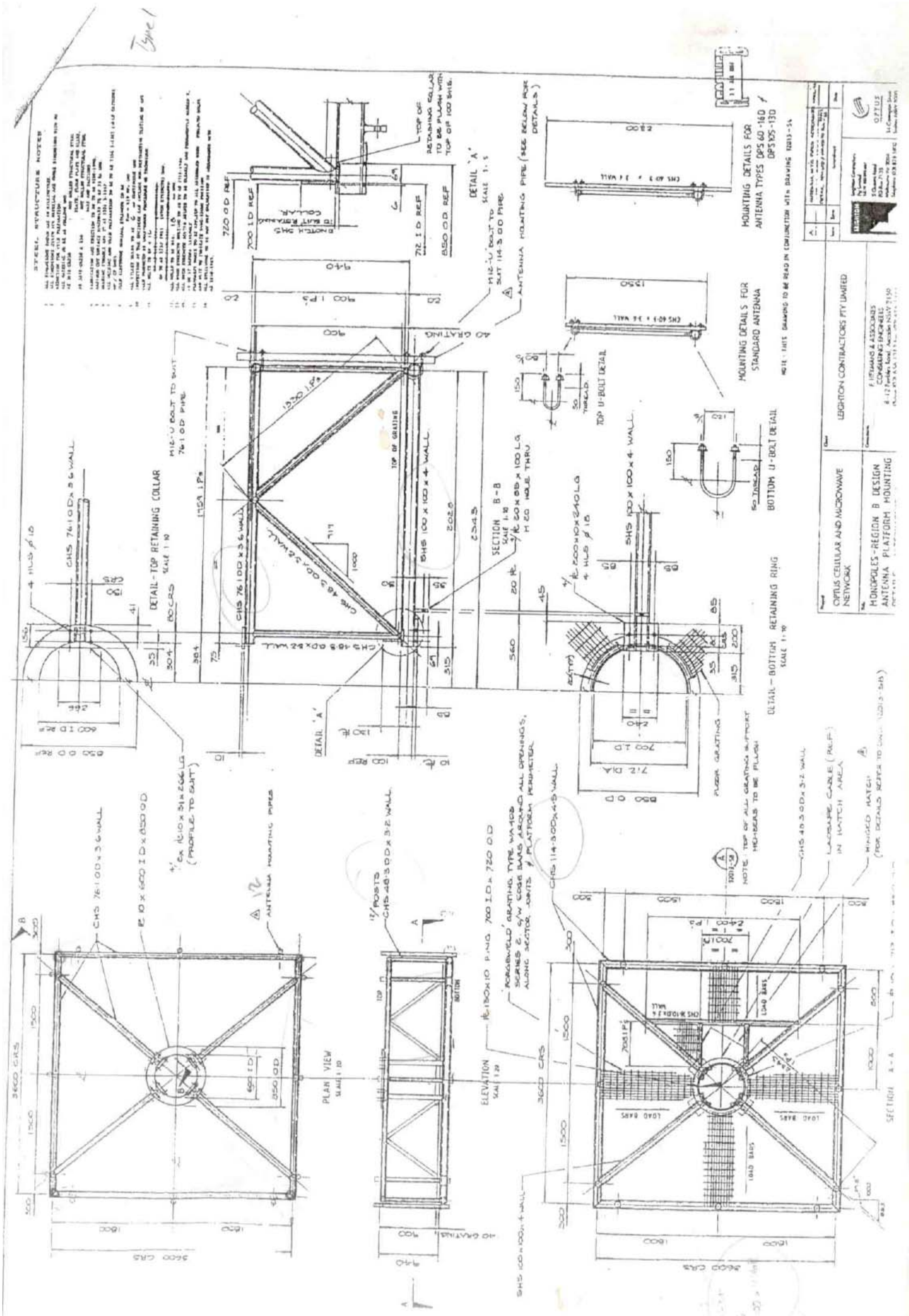

Triangular head frame

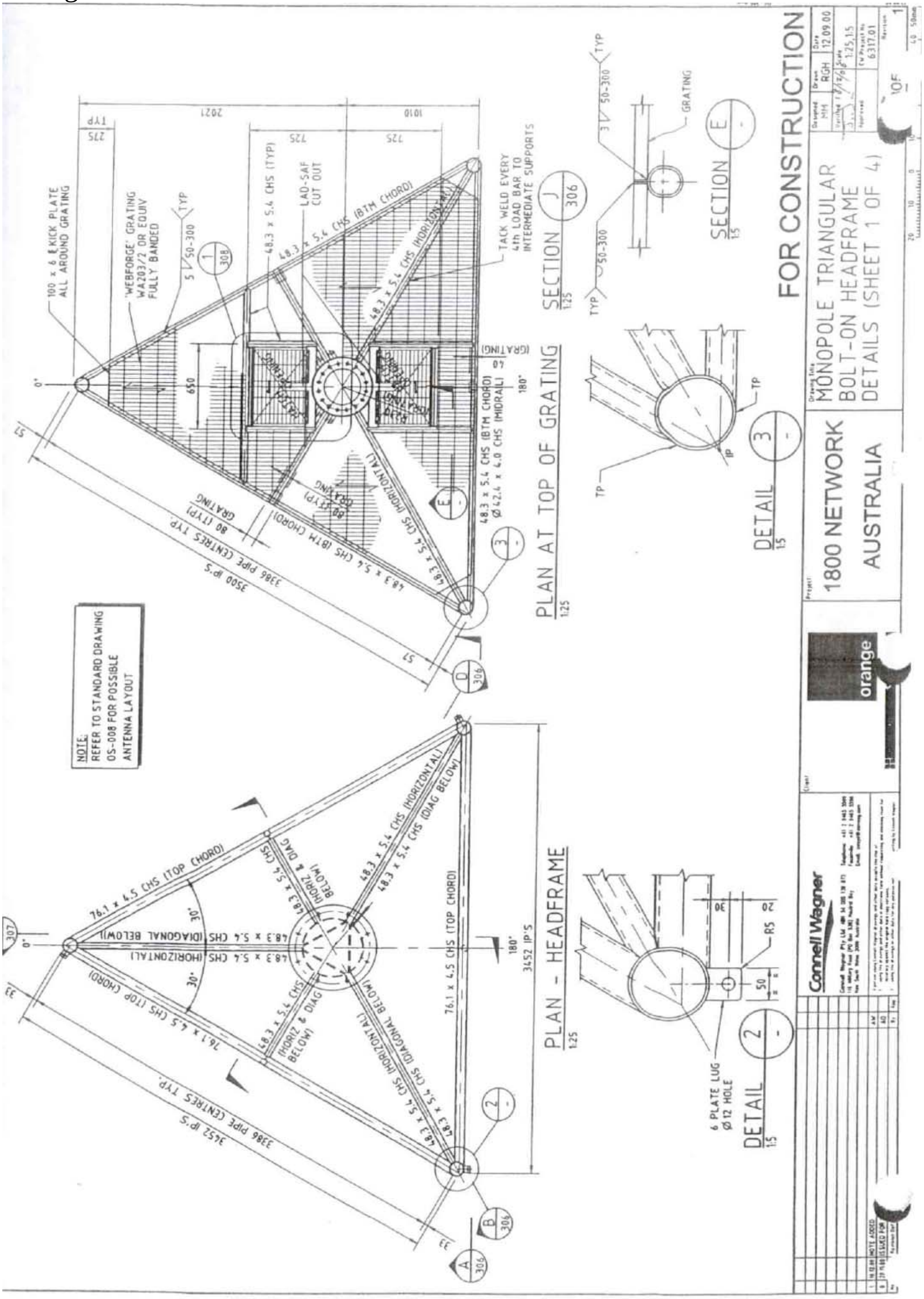

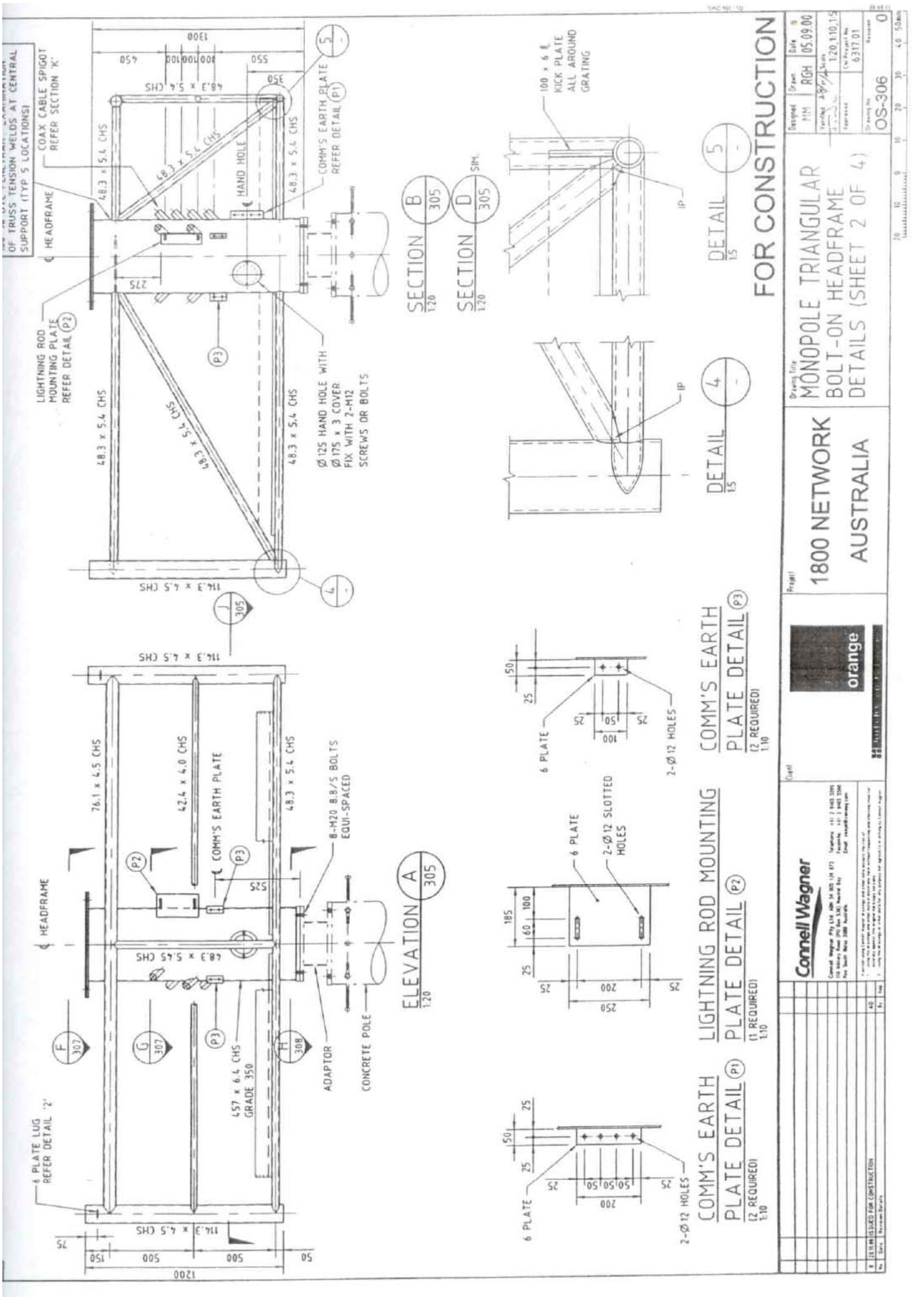
ELEVATION A 305
SECTION B 305
SECTION D 305
DETAIL 4
DETAIL 5
FOR CONSTRUCTION
COMM'S EARTH PLATE DETAIL (P1)
(2 REQUIRED)
1:10
LIGHTNING ROD MOUNTING PLATE DETAIL (P2)
(1 REQUIRED)
1:10
COMM'S EARTH PLATE DETAIL (P3)
(2 REQUIRED)
1:10
Connell Wagner
orange
1800 NETWORK
AUSTRALIA
MONOPOLE TRIANGULAR
BOLT-ON HEADFRAME
DETAILS (SHEET 2 OF 4)
OS-306

Circular head frame

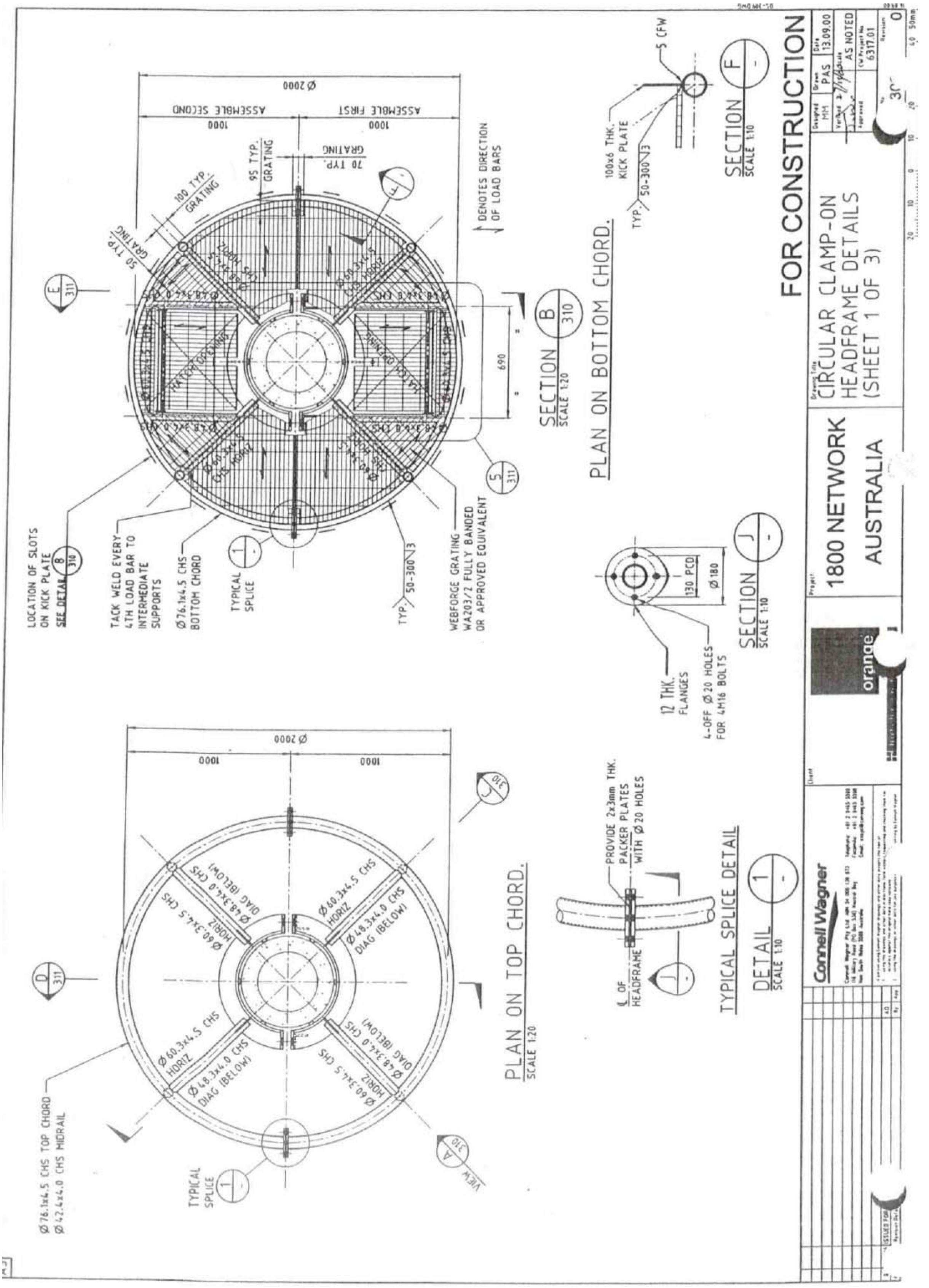

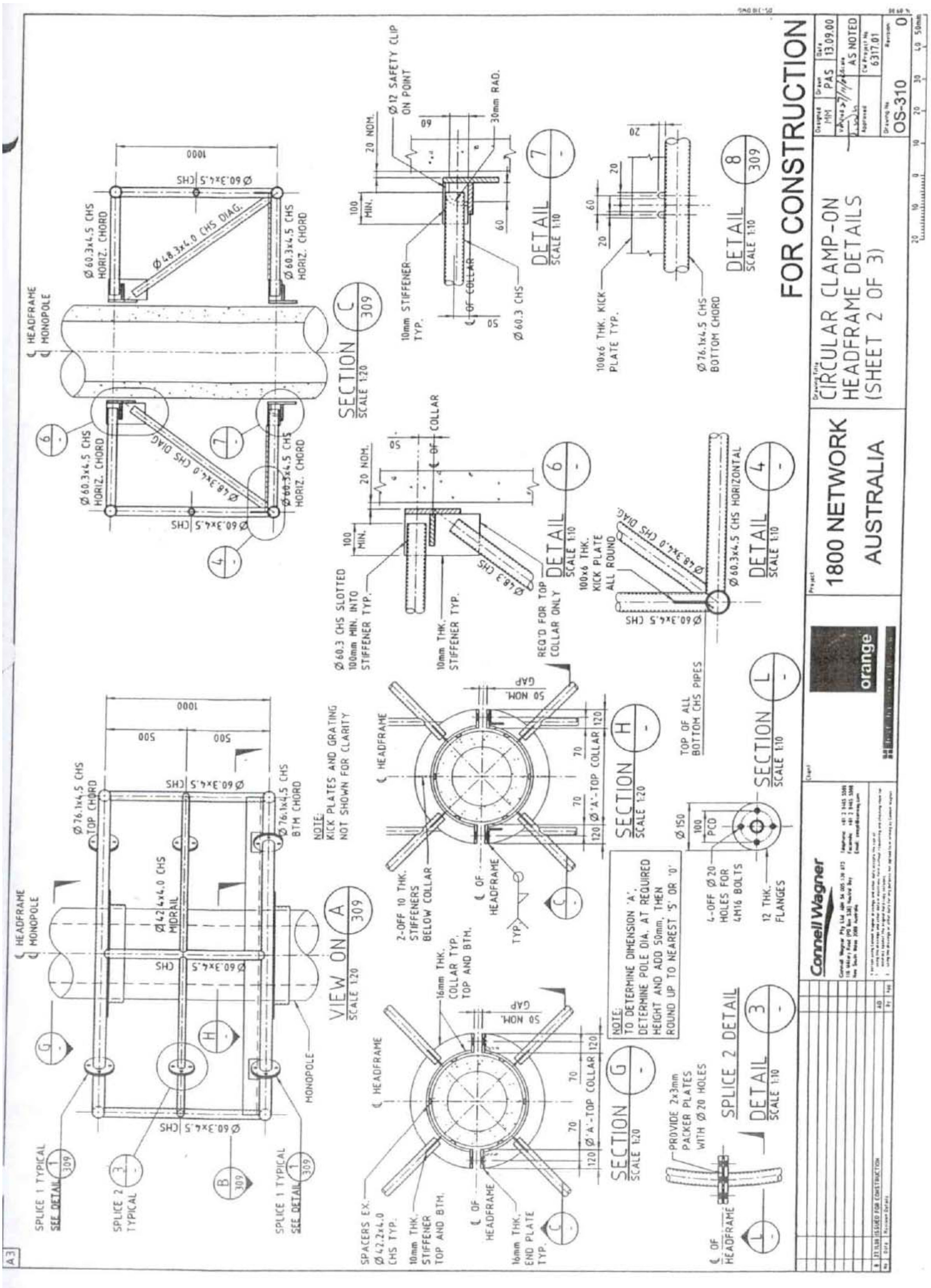
FOR CONSTRUCTION
CIRCULAR CLAMP-ON
HEADFRAME DETAILS
(SHEET 2 OF 3)
1800 NETWORK
AUSTRALIA
orange
Connell Wagner
OS-310
AS NOTED
13.09.00

Turret head frame

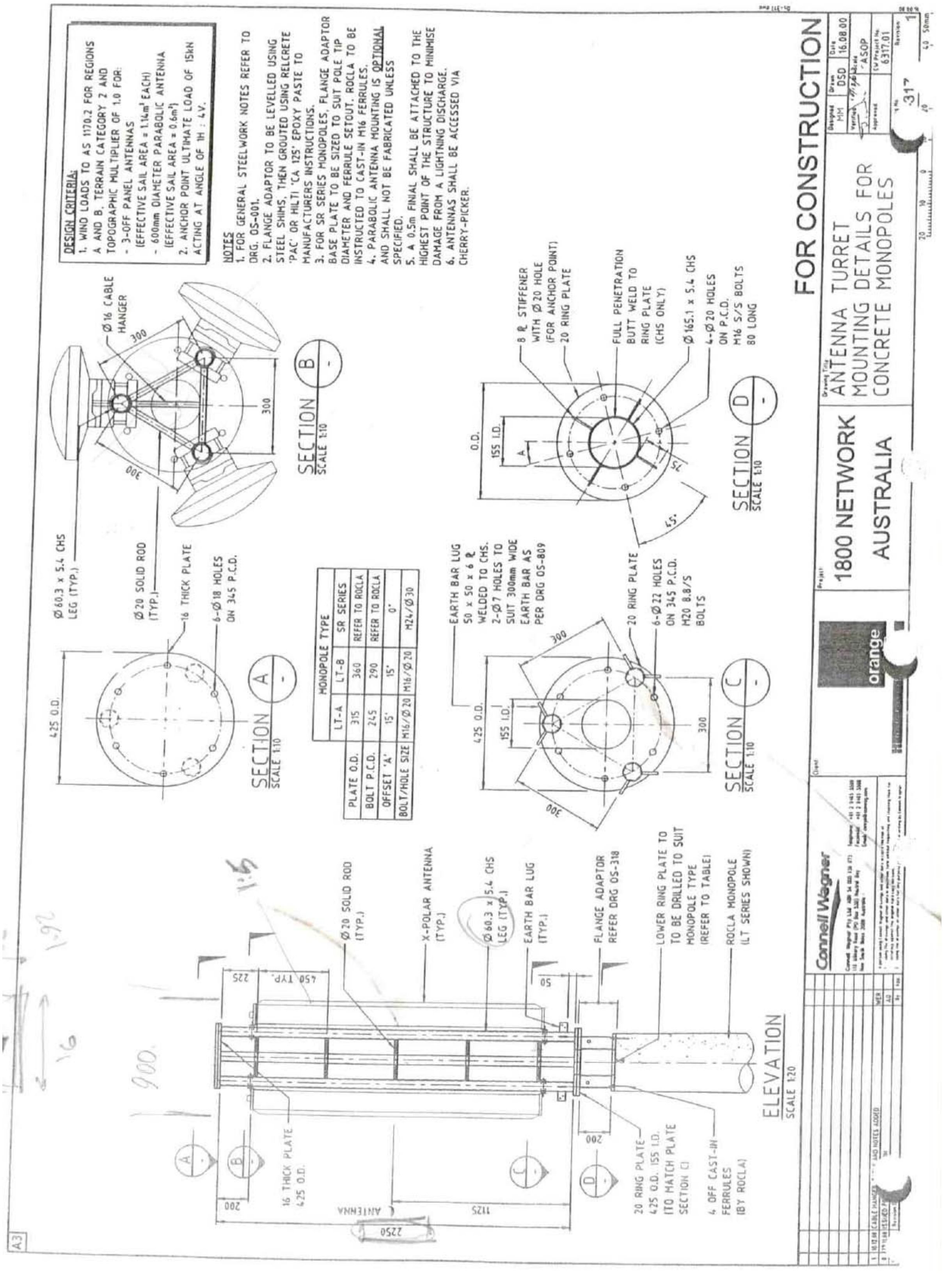

Mercedes head frame

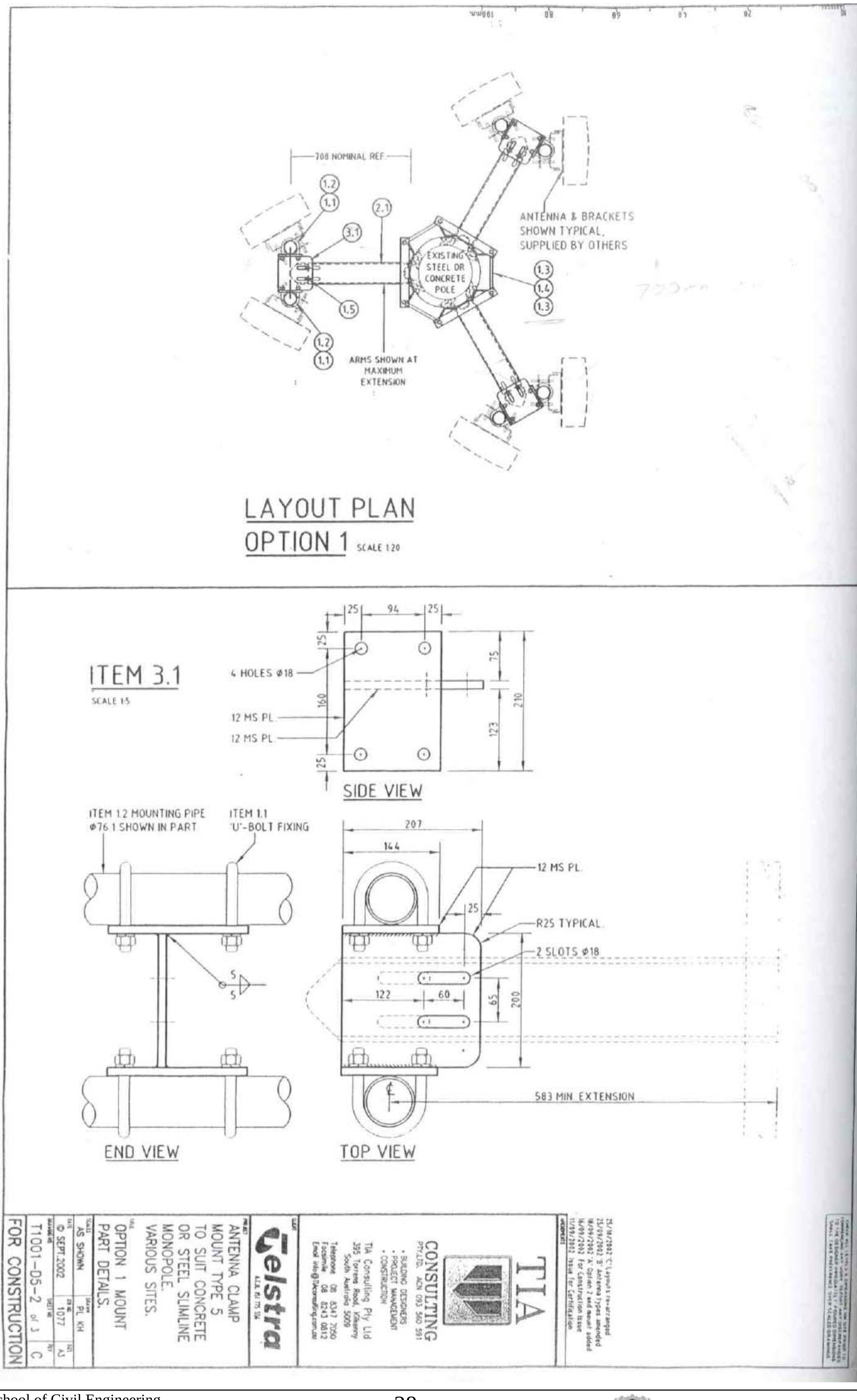

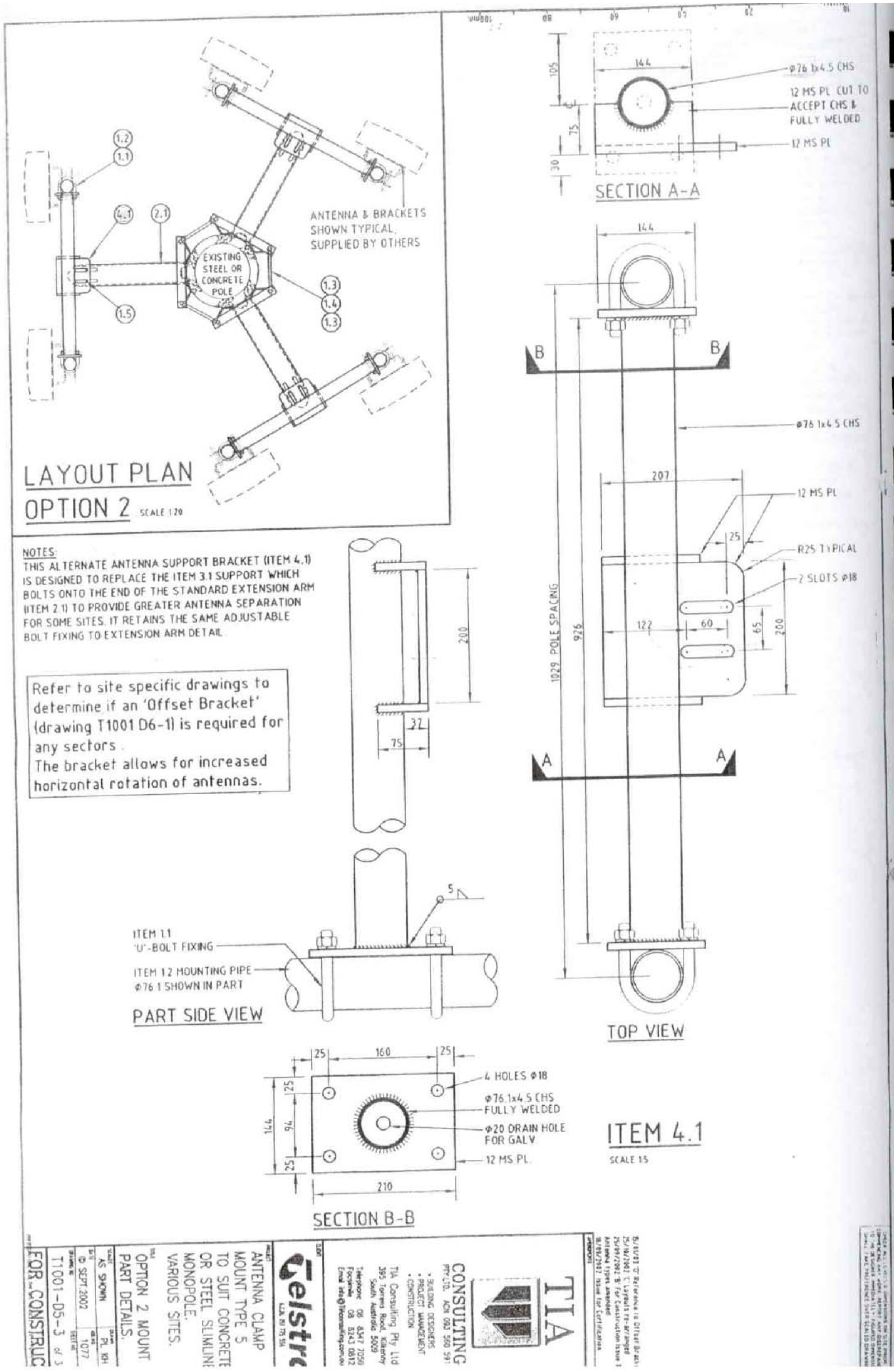
LAYOUT PLAN
OPTION 2 SCALE 1:20
ANTENNA & BRACKETS SHOWN TYPICAL, SUPPLIED BY OTHERS
EXISTING STEEL OR CONCRETE POLE
NOTES:
THIS ALTERNATE ANTENNA SUPPORT BRACKET (ITEM 4.1) IS DESIGNED TO REPLACE THE ITEM 3.1 SUPPORT WHICH BOLTS ONTO THE END OF THE STANDARD EXTENSION ARM (ITEM 2.1) TO PROVIDE GREATER ANTENNA SEPARATION FOR SOME SITES. IT RETAINS THE SAME ADJUSTABLE BOLT FIXING TO EXTENSION ARM DETAIL.
Refer to site specific drawings to determine if an 'Offset Bracket' (drawing T1001 D6-1) is required for any sectors.
The bracket allows for increased horizontal rotation of antennas.
SECTION A-A
φ76.1x4.5 CHS
12 MS PL CUT TO ACCEPT CHS & FULLY WELDED
12 MS PL
12 MS PL
R25 TYPICAL
2 SLOTS φ18
1029 POLE SPACING
ITEM 1.1 'U'-BOLT FIXING
ITEM 1.2 MOUNTING PIPE φ76.1 SHOWN IN PART
PART SIDE VIEW
TOP VIEW
4 HOLES φ18
φ76.1x4.5 CHS FULLY WELDED
φ20 DRAIN HOLE FOR GALV
12 MS PL
ITEM 4.1
SCALE 1:5
SECTION B-B
TIA CONSULTING
ANTENNA CLAMP MOUNT TYPE 5 TO SUIT CONCRETE OR STEEL SLIMLINE MONOPOLE. VARIOUS SITES.
OPTION 2 MOUNT PART DETAILS.
T1001-D5-3
FOR CONSTRUC